Wave attenuation in stands of common reed (*Phragmites australis*) and its consequences on sediment resuspension

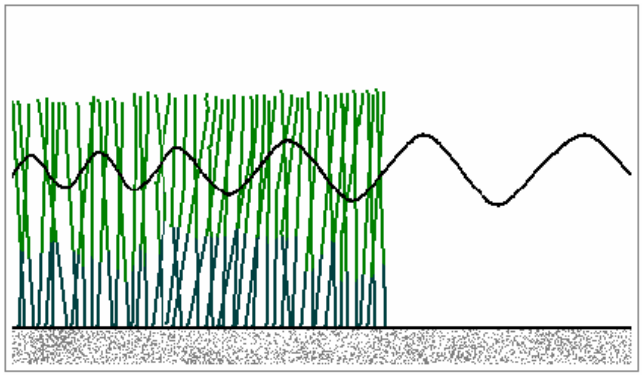

Per Falås
2007

Division of Water Resources Engineering
ISRN LUTVDG/TVVR-07/5004+82p
ISSN-1101-9824

Report TVVR 07/5004

Division of Water Resources Engineering,
Lund Institute of Technology, Lund University
Box 118
221 00 Lund
Sweden
Phone +46 46 222 000

Printed in Sweden

Summary

Title: Wave attenuation in stands of common reed (*Phragmites australis*) and its consequences on sediment resuspension

Author: Per Falås

Supervisor: Charlotta Borell Lövstedt, Division of Water Resources Engineering, Lund Institute of Technology, Lund University, Sweden

Examiner: Magnus Larson, Division of Water Resources Engineering, Lund Institute of Technology, Lund University, Sweden

Problem Definition: Common reed is found in near-shore areas of many European lakes, where it forms dense stands. As waves are influenced by obstacles along the wave path, water and sediment motions caused by waves are affected by these stands.

Objectives: This study aims to evaluate the effect of common reed stands on waves, evaluate the effect of common reed stands on wave induced sediment resuspension, test a model for wave attenuation by vegetation and discuss extensive common reed stands consequences to sediment induced turbidity in lakes.

Method: In order to evaluate the effects of common reed stands on waves and sediments, a field experiment was conducted in the common reed stands of a southern Swedish lake. The water surface displacement was measured simultaneously both within and outside these stands.

In order to test the model, it was adjusted to the prevailing wave regime with the drag coefficient.

Conclusions: A general decrease in significant wave height was observed along the wave path in the common reed stand. The average period on the other hand tended to increase along the wave path in the common reed stand.

Based on the applied analysis of the wave measurements, it was impossible to tell whether or not stands of common reed reduce the resuspension potential of wave regimes. This was not due to the wave measurements, but to a flaw in the analysis of the wave measurements. Visual observations indicated however that stands of common reed reduce wave breaking and thereby the resuspension potential of waves.

The modelled wave damping showed quite good agreement with the recorded wave damping and the drag coefficient seem to be dependent on Reynolds number.

Key words: *Phragmites australis*, Stands of common reed, Wave damping, Sediment resuspension, Shallow lakes, Alternative stable states.

Preface

This master's thesis was made at Lund Institute of Technology and it marks the end of my studies at the Environmental Engineering program at the same institute. I would like to take the opportunity to thank all the people who have contributed to this work. Firstly, I would like to thank my supervisor Charlotta Borell Lövstedt for her support and guidance. Secondly, I would like thank my field assistants Fredrik Magnusson, Jakob Falås and Per Åberg for their help during the field measurements. Lastly, I would like to thank the community of Revingeby for letting me use their boats.

Thank you All!

Lund 2007-03-18

Per Falås

Notation

a_x Horizontal water particle acceleration (m/s^2)
C Wave celerity (m/s)
C_d Drag coefficient (*dimensionless*)
C_g Group velocity (m/s)
C_{gb} Group velocity at the beginning of the wave path (m/s)
C_{ge} Group velocity at the end of the wave path (m/s)
C_m Inertia coefficient (*dimensionless*)
d Depth (m)
d_g Grain diameter (m)
d_{dsc} Wave energy loss per unit length of a cylinder caused by the drag force (N/s)
d_{50} Grain diameter at the fifty cumulative weight percent point (m)
$\overline{d}_{dsc}$ Time average wave energy loss per unit length of a cylinder caused by the drag force (N/ms)
D Cylinder diameter (m)
D_A Wave energy loss per unit surface area (N/ms)
D_B Wave energy loss per unit surface area caused by bottom friction (N/ms)
D_V Wave energy loss per unit surface area caused by vegetation (N/ms)
D_* Dimensionless grain size (*dimensionless*)
$\overline{D}_{dac}$ Time average wave energy loss per unit area caused by the drag force acting on an array of cylinders (Nm/s)
$\overline{D}_{dsc}$ Time average wave energy loss per cylinder caused by the drag force (Nm/s)
E Wave energy per unit crest width (N)
E_k Kinetic wave energy per unit crest width (N)
E_p Potential wave energy per unit crest width (N)
$\overline{E}$ Wave energy per unit surface area (N/m)
$\overline{E}_b$ Wave energy per unit surface area at the beginning of the wave path (N/m)
$\overline{E}_e$ Wave energy per unit surface area at the end of the wave path (N/m)
f Wave force acting on a cylinder per unit length (N/m)
f_i Inertia force per unit length of cylinder (N/m)
f_D Drag force per unit length of cylinder (N/m)
f_w Wave friction factor (*dimensionless*)
F Wave energy flux per unit crest width (N/s)
g Acceleration of gravity (m/s^2)
h Wave height (m)
h_b Wave height at the beginning of the wave path (m)
h_e Wave height at the end of the wave path (m)
H Significant wave height (m)
Hm Significant wave height at movable station (m)
H_{rms} Root mean-square wave height (m)
$H0$ Significant wave height at fixed station (m)
k Wave number (m^{-1})
L Wave length (m)
m Number of recordings of the water surface elevation within a measurement cycle (*dimensionless*)

n Rank of wave (*dimensionless*)
n_g Dimensionless factor related to the group velocity (*dimensionless*)
N Total number of waves within a wave record (*dimensionless*)
N_c Number of cylinders per unit area (m^{-2})
R_b Reynolds Number related to the bottom (*dimensionless*)
Re Reynolds number related to the reed (*dimensionless*)
t Time elapsed from a set time (*s*)
T Wave period (s)
u Horizontal water particle velocity (*m/s*)
u_b Peak horizontal velocity just above the bottom boundary layer (*m/s*)
u_{bcr} Critical orbital velocity just above the bottom boundary layer (*m/s*)
u_{max} Peak horizontal water particle velocity at the still water level (*m/s*)
x Distance from a fixed location (*m*)
z Distance from the still water level (*m*)
ζ Vertical water particle displacement (*m*)
η Water surface elevation (*m*)
θ Phase angle (*dimensionless*)
θ_{cr} Shields parameter (*dimensionless*)
ν Viscosity of water (m^2/s)
ξ Horizontal water particle displacement (*m*)
ξ_b Maximum horizontal water particle excursion just above the bottom boundary layer (*m*)
ρ Density of water (kg/m^3)
ρ_s Density of sediment (kg/m^3)
σ Wave frequency (s^{-1})
τ_{cr} Critical bed shear stress (N/m^2)
τ_f Form drag (N/m^2)
τ_s Skin friction (N/m^2)
τ_t Sediment transport (N/m^2)
τ_{ws} Peak skin friction caused by waves (N/m^2)
τ_0 Bed shear stress (N/m^2)

Table of content

1 Introduction

Waves propagating through vegetation beds lose energy due to the interaction with vegetation. The wave energy dissipation depends on both vegetation and wave characteristics. (Mendez and Losada, 2004). A number of models concerning wave energy dissipation in vegetation stands have been presented and some of them have been tested in wave tanks. Information about how well the models describe wave energy dissipation in natural occurring vegetation stands is scarce. Actually, very few field measurements on wave propagation through vegetation stands have been performed. To compensate for this lack of information, a field experiment has been carried out in Lake Krankesjön to obtain information about how stands of emergent macrophytes affect waves. The results, concerning wave attenuation, obtained from the field experiment will be compared with the ones generated by a model.

An important aspect of wave propagation through shallow water is resuspension of sediments (Teeter et al., 2001). Resuspension caused by waves is generally most pronounced in shallow areas with high wave energy input and low vegetation cover. Emergent macrophytes that form dense stands in shallow water can stabilize sediments and reduce the wave energy input, to areas behind the stands outer edge. Dense stands of emergent macrophytes can therefore reduce resuspension and act as erosion barriers along the shoreline.

The field experiment, concerning wave attenuation by vegetation, is conducted on common reed (*Phragmites australis*). Common reed is of great interest for several reasons. It is common and widely distributed (Haslam, 1972). It has a growth characteristic and growth distribution that can reduce resuspension or at least shoreline erosion. Coops et al. (1996) showed in a wave tank experiment that common reed reduce bank erosion and Ostendorp et al. (1995a) observed that the decline of common reed, in several Central European lakes, led to increased shoreline erosion.

Lake ecosystems are affected by sediment resuspension (Horppila and Nurminen, 2001). Resuspension of sediments increase the turbidity, which has a great impact on shallow lakes. It is assumed that shallow and moderately eutrophic lakes can occur in two alternative stable states, a clear water sate and a turbid state. The clear water state is characterized by high abundance of submerged macrophytes and high water transparency. The turbid state is characterised by low abundance of submerged macrophytes, high density of phytoplankton and low water transparency. Some shallow lakes do switch back and forth between these two states and the intervals between two switches are generally of many years. How these changes in water transparency do come about is not fully understood. It is however suggested that changes in the lake can reinforce each other and bring about a long term change in water transparency. It is also supposed that a change in resuspension rate can be reinforced through the interaction with other factors (such as the amount of phytoplankton, submerged macrophytes, suspended solids and dissolved nutrient) and thereby generating a long term change in water transparency. Lake Krankesjön is a shallow and moderately eutrophic lake in southern Sweden, which has switched between turbid states and clear water states. Dense and extensive stands of common

reed are found in Lake Krankesjön at almost all near-shore areas. It can be assumed that these stands have great impact on sediment resuspension.

1.1 Objectives of the study

This study aims to evaluate the effects of common reed stands on waves, evaluate the effect of common reed stands on wave induced sediment resuspension, test a model for wave attenuation by vegetation and discuss extensive common reed stands consequences to the sediment induced turbidity in lakes.

1.2 Procedure

In order to meet the objectives of the study, a field experiment concerning wave attenuation was conducted in the common reed stands of Lake Krankesjön and in a control area without common reed. The field experiment support us with accurate information about the water surface elevation along a transect, perpendicular to the reed stands outer edge. The field experiment, concerning wave attenuation, serves as the backbone of the study. Chapter 2 contains background information about Lake Krankesjön, resuspension, alternative stable in shallow lakes and common reed. This background and the results from the field experiment are later used to discuss common reed stands consequences on sediment induced turbidity in lakes. Chapter 3 gives a short introduction to linear wave theory. This introduction serves as starting point for the derivation and formulation of the wave energy dissipation and resuspension formulas presented in chapter 4. This is followed by descriptions of the field experiment, analysis method, wave attenuation models and resuspension calculations. The results obtained from the field experiment, wave attenuation models and resuspension calculations are given in chapter 8. These results are thereafter discussed. Finally, conclusions and recommendations for further studies are given in chapter 10 and 11.

2 Background

2.1 Lake Krankesjön

Lake Krankesjön is situated in southern Sweden, where the winds are mostly westerly and southerly (Jönsson et al., 2005).

The lake area is $2.9 km^2$ the mean depth is $0.7 m$ and the maximum depth is $3 m$. Krankesjön can be described as a shallow and moderately eutrophic lake, and it shifted from a turbid state to a clear water states in the mid-1980s (Blindow et al., 2002), and it has remain in this state ever since. Shifts between the two alternative stable states have also been observed before the 1980s. The lake topography and the extension of the reed stand can be seen in figure 1.

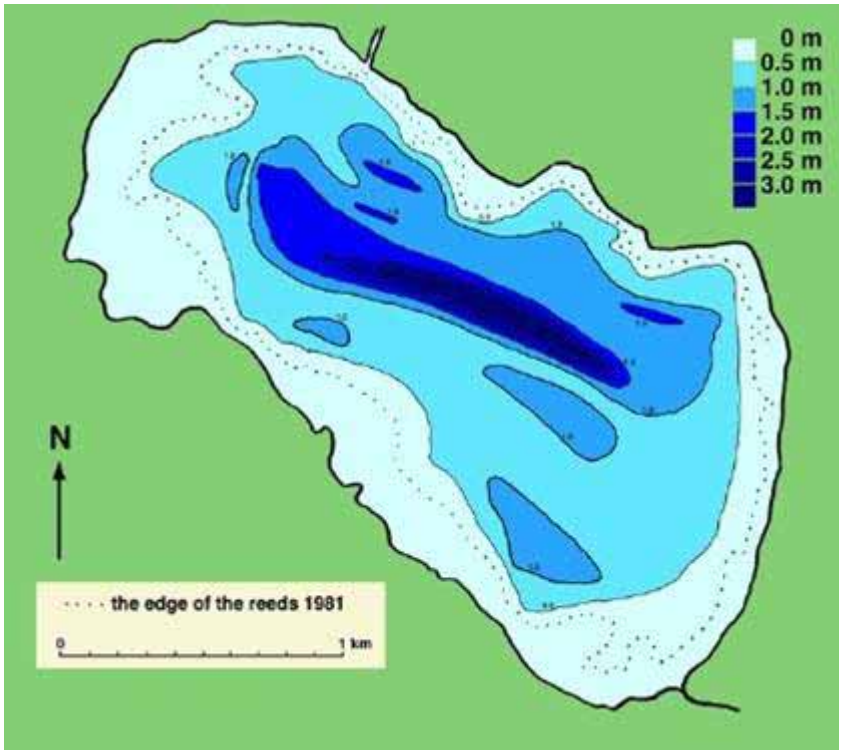

Figure 1. Map over Lake Krankesjön. (Link 1)

Forests are found at the south western parts of the lake and at the eastern parts of the lake. Apart from this the lake is mostly surrounded by open terrain. (Lantmäteriverket, 1999)

2.2 Resuspension

Resuspension is the process through which sediments are lifted from the bottom into the water column. Resuspension occurs as a result of the water motions at the sediment surface. Water motions at the sediment surface generate a bed shear stress and if this bed shear stress exceeds the critical shear stress resuspension might occur. The critical shear stress is the lowest bed shear stress for a given sediment that is required to bring sediment particles in motion.

Both waves and currents can generate water movements at the sediment surface. Water currents are acting over long periods, which generate a growth in boundary layer thickness and a decline in the velocity gradient within the boundary layer. Wave induced orbital velocities are constantly changing direction. The boundary layer does therefore not have time to grow and the velocity gradient within the boundary layer remains steep. Consequently, the velocity of a current must be much larger than the wave induced orbital velocity in order to generate the same bed shear stress. (Luettich et al., 1990) For this reason it is assumed that water currents have little effect on resuspension in lakes. Currents are however important to the horizontal transport of suspended sediments, while waves contribute little to this process. Biological activity at the sediment surface is also known to cause resuspension. Benthivorous fish such as bream (*Abramis brama*) can resuspend sediments as they feed (Hansson et al., 1998).

The amount of suspended sediments in the water mass increases as long as the resuspension rate exceeds the sedimentation rate. The sedimentation rate increases with the volume per area ratio and the density of the sediment particles. A small particle can therefore remain in suspension for a longer period than a large particle with the same shape and density.

The critical shear stress is sediment specific. In non-cohesive sediments the critical shear stress is determined by friction between the sediment particles and it is therefore generally higher for large particles with high density than small particles with low density. In cohesive sediments the critical shear stress is mainly caused by cohesive forces. The critical shear stress is however not only affected by friction and cohesive forces, but also by biotic factors such as algae and macrophytes (Widdows and Brinsley, 2002).

Wave induced resuspension can be important to water transparency in shallow lakes, where large areas might be affected by wave induced water motions at the sediment surface. The water transparency in deep lakes on the other hand is rarely influenced by wave induced resupension, because only shallow areas can be affected. Resuspension caused by waves might be important to the vegetation community, which will be discussed in detail in chapter 2.3.

2.3 Alternative stable states in shallow lakes

Shallow and moderately eutrophic lakes are supposed to have two alternative stable states, a clear water state and a turbid state. The clear water state is characterised by high abundance of submerged macrophytes, low algae density and low turbidity. The

turbid state is characterised by low abundance of submerged macrophytes and high algae density and high turbidity. Some shallow lakes switch between these two states. The exact mechanism behind these shifts is not known, but the interaction between turbidity and macrophytes are however assumed to play a key role (figure 2).

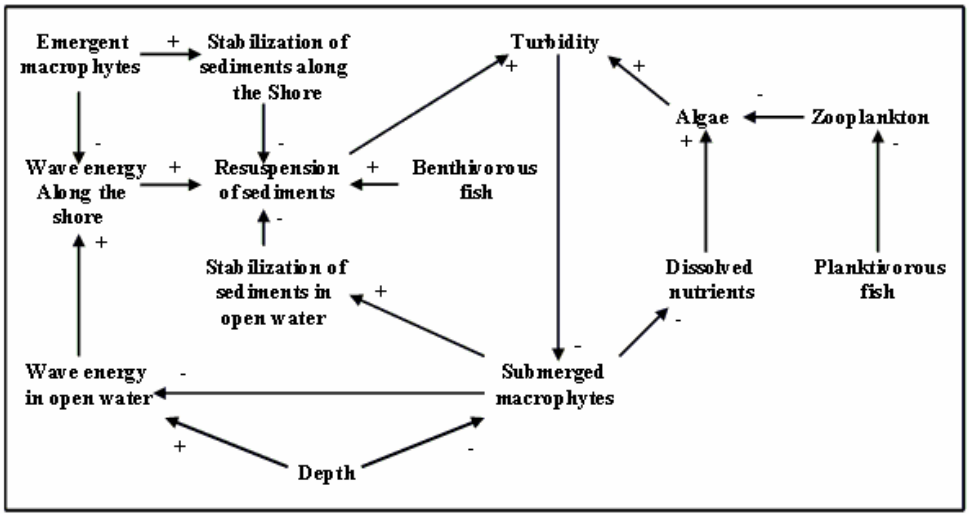

Figure 2. The main factors and interactions expected to be in control of the water transparency state in lakes with alternative stable states.

Most studies concerning macrophytes impact on alternative stable states in shallow lakes have been restricted to submerged macrophytes. Submerged macrophytes can only grow down to a light critical depth, which is turbidity dependent. Turbidity is affected by submerged vegetation through a number of mechanisms.

- Submerged macrophytes compete with algae for dissolved nutrients, which affects the algae induced turbidity.

- Submerged macrophytes provide zooplankton with protection against planktivorous fish. A change in zooplankton density affects the grazing on algae, which in turn affects turbidity.

- Submerged macrophytes stabilize sediments, through coverage of sediments and with their roots. This affects bentivorous fish access to the sediments and thereby resuspension. The vegetation cover does also affect the water velocity at the sediment surface and thereby resuspension. Both water motions at the sediment surface and bentivorous fish affect sediment resuspension and thereby turbidity.

- Submerged macrophytes can dissipate wave energy, which affects the resuspension potential of the wave and thereby turbidity.

Turbidity is not only affected by submerged macrophytes, it does also affect submerged macrophytes through the alteration of the subsurface light regime. A change in turbidity or submerged macrophyte abundance can therefore be reinforced through all the above mentioned mechanisms.

Emergent macrophytes are generally less sensitive to changes in the subsurface light regime, than submerged macrophytes. Emergent macrophytes can therefore reduce sediment resuspension over a larger turbidity range. Another difference between submerged and emergent macrophytes is that submerged macrophytes absorb nutrients from both the sediment and the water, while emergent macrophytes only absorb nutrients from the sediment. Consequently, there is no competition between algae and emergent macrophytes for dissolved nutrients. Submerged macrophytes have therefore stronger impact on algae induced turbidity, than emergent macrophytes. Emergent macrophytes do however affect turbidity through a number of resuspension related mechanisms.

- Emergent macrophytes stabilize sediments with both their above ground parts, leafs and steams, and below ground parts, roots and rhizomes. The below ground parts reinforce the sediment, which can affect shore erosion. The above ground parts affect the wave induced orbital velocities, where the horizontal orbital velocity just above the sediment surface has great impact on resuspension. Both the above and the below ground parts can therefore affect the amount of suspended solids in the lake.

- Emergent macrophytes dissipate wave energy, which affect the resuspension potential of waves and thereby the amount of suspended solids in the lake.

- Emergent macrophytes reduce wind energy with their above surface parts, which affects wave energy and thereby the resuspension potential of waves. This does in turn affect the amount of suspended solids in the lake.

Turbidity is affected by emergent macrophytes, but emergent macrophytes are not very sensitive to alterations of the subsurface light regime caused by turbidity. Turbidity does therefore generate a stronger feedback system with submerged macrophytes, than it does with emergent macrophytes.

The water depth is important to the interaction between waves, macrophytes and turbidity, for several reasons.

- Submerged macrophytes can only grow down to a light critical depth, which is turbidity dependent.

- Emergent macrophytes can only grow down to a growth critical depth.

- Waves can only affect resuspension if the water motions caused by the waves reach down to the bottom.

- Wave energy is dissipated through bottom friction if the water motions caused by the wave reach down to the bottom.

- Wave energy is dissipated through the interaction with submerged macrophytes if the water motions caused by the wave reach down to the submerged macrophytes.

- Wave energy is dissipated through the interaction with emergent macrophytes if emergent macrophytes are present above the growth critical depth.

Shallow lakes have a topography that supports the interaction between waves, vegetation and turbidity over large areas. Shallow lakes are therefore more sensitive to changes in turbidity and vegetation than deep lakes.

2.3 Common reed and its effect on resuspension

Common reed (*Phragmites australis*) is an emergent macrophyte that growths on water saturated and submerged soils. It has an extensive root system (Haslam,1958) and rigid aerial stems. Common reed has been used to stabilize river and canal banks. It is suggested that roots and stems of common reed reduce bank erosion through different mechanisms. The roots reinforce the sediments, while the steams attenuate wave energy as the waves propagate through the stand. It can be assumed that these mechanisms also affect resuspension in lakes. The importance of common reed to sediment stabilization is not only dependent on its horizontal and vertical extension, but also on incident wave height, water depth and sediment type. Türker et al. (2006) studied, in a wave tank experiment, how a beach profile responded to waves that had propagated through a stand of defoiled common reed. The experiment showed that the response of the beach profile increased with an increase in initial wave height, a decrease in vegetation area and a decrease in sediment particle diameter. The variation in erosion and resuspension caused by initial wave height and vegetation area is directly linked to wave energy. The resupension potential of waves do consequently increases with wave energy. Waves propagating through stand of common reed lose energy and thereby resuspension potential.

Extensive stands of common reed can be assumed to reduce the resuspension potential of waves over large areas. If such stands occur in shallow lakes with two alternative stable states, they can be assumed to have a key role in the maintenance of the clear water state as well as supporting a switch from the turbid state. In Lake Krankesjön is nor the turbid or clear water state known to affect the distribution of common reed. This does however not imply that the stands of common reed in Lake Krankesjön have no effect on the turbid or the clear water state.

2.4 Other studies of the interaction between waves and vegetation

It is generally agreed that aquatic vegetation increases the water flow resistance and that water flows can be a stress factor to aquatic vegetation. Stress induced by water motions on vegetation have been studied by Ostendorp (1995), who investigated how waves cause mechanical damage to common reed. According to Ostendorp (1995), it is generally assumed that reed fronts adjacent to large areas of open water are in equilibrium with the mechanical damage caused by waves and drifting matter.

Emergent macrophytes are of interest to waterway engineering, because emergent macrophytes can be used to reduce canal bank erosion through damping of waves by the above ground parts and stabilization of the sediments by the below ground parts. The possibilities of canal bank stabilization through planting of common reed and two other emergent macrophytes in a newly reconstructed canal bank have been studied in a field experiment by Beglin and Caffrey (1996). Coops et al. (1996) showed in a wave tank experiment that canal bank erosion caused by waves is reduced, when common reed is present.

Several models concerning wave attenuation by vegetation have been presented. Kobayashi et al. (1993) and Dalrymple et al. (1984) presented models where swaying motions of plants were neglected. In the model presented by Dalrymple et al. (1984), it is however suggested that the effect of plant motions can be compensated for through an alteration of the drag coefficient. Asano et al. (1992) on the other hand included the interaction between waves and the swaying motions of plants in the model. Both Asano et al. (1992) and Kobayashi et al. (1993) compared the modelled damping with the wave damping obtained from a wave tank experiment with artificial kelp, i.e. plastic straps. Massel et al. (1999) did not only present a model of wave attenuation in mangrove forests but also a field study on wave attenuation in mangrove forests. The results from the model were however not compared with the results obtained from the field experiment. Field studies on wave attenuation by vegetation have also been made in a salt marsh (Möller, 2006).

3 Wave mechanics

Waves do not only affect the surface elevation, but also water motions beneath surface. These subsurface motions are however much harder to measure than the changes in water level. The wave characteristics in figure 3 describe the shape and elevation of the water surface. These parameters along with the wave period, which is the time it takes for a wave to travel one wave length, can be used to model surface and subsurface water motions.

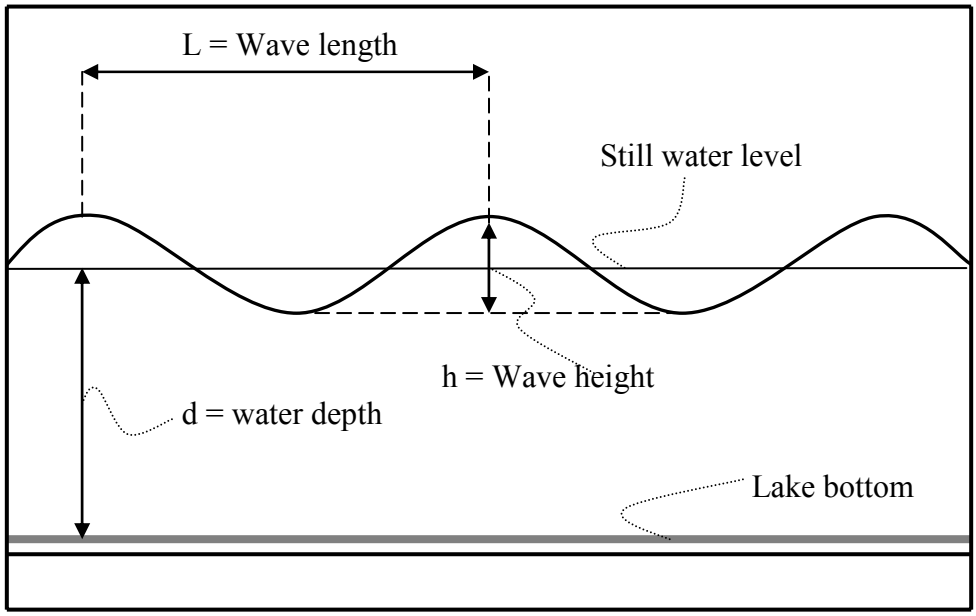

Figure 3. Wave characteristics

Many wave theories have been presented, but only a few have found a wide range of application. One of the most widely used theories is linear wave theory, which benefits from fact that it is easy to use and that it gives acceptable approximation of waves over a large range of wave conditions (SPM, 1984). All equations in chapter 3 are based on linear wave theory.

3.1 Surface parameters

Waves generate changes in surface elevation, and these changes can be measured or estimated from an adequate wave theory. At the field experiment in Lake Krankesjön the water surface displacement over time is measured. These measurements can be used to estimate wave heights and wave periods. When these parameters and the water depth are known linear wave theory can be used estimate other parameters of interest.

The wave length, L, (m) is dependent on water depth and wave period. The wave length can be iterated from the following equation

$$L = \frac{gT^2}{2\pi}\tanh\left(\frac{2\pi d}{L}\right) \quad (1)$$

where T is the wave period (s), d is the water depth (m) and g is the acceleration of gravity (m/s^2).

The wave celerity, C, (m/s) is the speed by which a single wave moves and it can be calculated by

$$\mathrm{C} = \frac{L}{T} \quad (2)$$

The single wave does not always propagate with the same speed as wave group. The group velocity, C_g, (m/s) is the speed by which wave energy is transmitted in the direction of wave propagation and it can be expressed as

$$C_g = n_g C \quad (3)$$

where n_g is a dimensionless factor, which is dependent on the water depth and the wave length. The dimensionless factor n_g can be calculated by

$$n_g = \frac{1}{2}\cdot\left(1 + \frac{4\pi d / L}{\sinh(4\pi d / L)}\right) \quad (4)$$

3.2 Subsurface parameters

Subsurface water motions generated by waves are of paramount importance to the interaction of waves with sediment and vegetation. Generally, water particles move in elliptical orbits in shallow and transitional water, and in circular orbits in deep water (figure 4). Deep water waves are not affected by the bottom, while shallow and transitional water waves are. It is this interaction with the bottom that causes water particles to move in elliptical orbits.

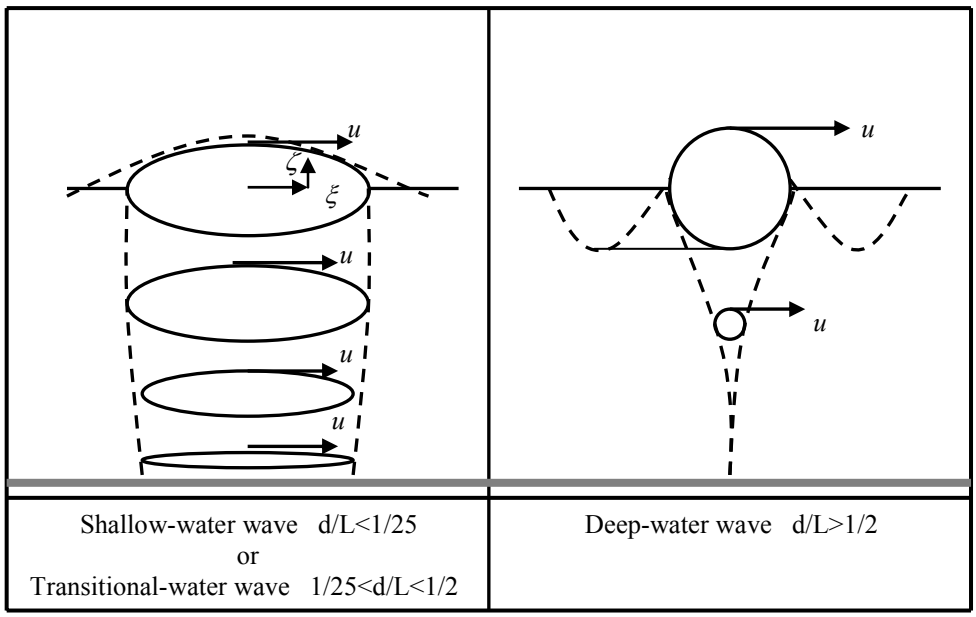

Figure 4. Water particle orbits for shallow, transitional and deep water waves.

According to linear wave theory water particles moves in closed orbits with a fixed centre. The water particle displacement is the distance from the centre of the wave orbital to the edge of the wave orbital, where the water particle displacement can be divided into a horizontal part, ξ, and vertical part, ζ. The horizontal water particle displacement (m) can be expressed as

$$\xi = -\frac{hgT^2}{4\pi L}\frac{\cosh\left[2\pi\left(z+d\right)/L\right]}{\cosh\left(2\pi d/L\right)}\sin\left(\frac{2\pi x}{L}-\frac{2\pi t}{T}\right) \tag{5}$$

where h is the wave height (m), z is the distance from the still water level (m), x is a horizontal distance from a fixed location (m) and t is the time elapsed from set time (t).

The horizontal water particle velocity, u, (m/s) is obtained by differentiating the horizontal water particle displacement with respect to t.

$$u = \frac{d\xi}{dt} = \frac{h}{2}\frac{gT}{L}\frac{\cosh\left[2\pi\left(z+d\right)/L\right]}{\cosh\left(2\pi d/L\right)}\cos\left(\frac{2\pi x}{L}-\frac{2\pi t}{T}\right) \tag{6}$$

By differentiating the horizontal water particle velocity with respect to t, the horizontal water particle acceleration, a_x, (m/s^2) is obtained.

$$a_x = \frac{du}{dt} = \frac{hg\pi}{L}\frac{\cosh\left[2\pi\left(z+d\right)/L\right]}{\cosh\left(2\pi d/L\right)}\cos\left(\frac{2\pi x}{L}-\frac{2\pi t}{T}\right) \tag{7}$$

As seen from equations 5, 6 and 7 there is a decline in horizontal water particle, displacement, velocity and acceleration with increasing distance below the still water level.

3.3 Wave energy

Wave energy is transmitted in the direction of wave propagation and the energy of a wave can be estimated if depth, wave height and wave period are known. The total wave energy is the sum of the kinetic and the potential energy. The amount of energy of a wave per unit crest width is given by

$$E = E_k + E_p = \frac{\rho g h^2 L}{16} + \frac{\rho g h^2 L}{16} = \frac{\rho g h^2 L}{8} \tag{8}$$

where E is the energy per unit crest width (N), E_k is the kinetic energy per unit crest width (N), E_p is the potential energy per unit crest width (N), ρ is the density of the water (kg/m^3).

The wave energy per unit surface area, $\overline{E}$, (N/m) can be calculated if wave energy is divided by the wave length.

$$\overline{E} = \frac{E}{L} = \frac{\rho g h^2}{8} \tag{9}$$

The wave energy per unit surface area will also be referred to as wave energy density. The wave energy flux is the rate of wave energy transfer in the direction of wave propagation and the average wave energy flux per unit crest width, $\overline{F}$, (N/s) can be calculated by

$$\overline{F} = C_g \overline{E} \tag{10}$$

3.4 Shoaling

Shoaling is a mechanism that affects the wave height and it occurs when waves propagates into shallower water. Shoaling can be derived from an energy balance along the wave path, equation 11.

$$C_{gb} \overline{E}_b = C_{ge} \overline{E}_e \tag{11}$$

where $\overline{E}_b$ and $\overline{E}_e$ are the wave energy densities at the beginning and the end of the wave path (N/m), C_{gb} and C_{ge} are the group velocities at the beginning and the end of the path (m/s).

The energy balance above is valid for steady state conditions if no wave energy is added or removed and the wave crests are parallel to the bottom contours. Since the group velocity is depth dependent, the wave energy density must be depth dependent too, in order to satisfy the energy balance (equation 11). The only part of the wave energy density that can vary is however the wave height. Subsequently, the wave heights will be affected, when the waves travels into shallower water. Substitution of equation 9 in equation 11 and isolation of the wave heights gives

$$\frac{h_e}{h_b} = \sqrt{\frac{C_{gb}}{C_{ge}}} \tag{12}$$

where h_b is the wave height at the beginning (m) of the wave path and h_e is the wave height at the end of the wave path (m).

The alteration of the wave height caused by the depth dependence of the group velocity is called shoaling.

4 Wave energy dissipation in near-shore areas and resuspension

Dissipation of wave energy is most pronounced in near-shore areas, where the wave energy is dissipated through breaking, bottom friction and interaction with vegetation. The most efficient way of wave energy dissipation is wave breaking, which occurs in near-shore areas, when the ratio between water depth and wave height becomes sufficiently low. Wave breaking results in water turbulence that can lift sediments. Propagation of waves through vegetation causes dissipation of energy, which leads to that less wave energy will be dissipated through breaking, if breaking occurs at all. Vegetation stands that have large enough horizontal and vertical extension will be able to prevent wave breaking. If the reed stand has such an extension, wave breaking can be omitted from energy balance. The mechanisms by which wave energy can be dissipate are then limited to bottom friction and interactions with the reed stand.

The wave energy balance is (Dean and Bender, 2006)

$$\frac{\partial\left(C_g\,\overline{E}\right)}{\partial x}+\frac{\partial\overline{E}}{\partial t}+D_A=0 \tag{13}$$

where x (m) is the length in the direction of wave propagation, t is the time (s) and D_A is the dissipated energy per unit area (N/ms).

The wave energy is assumed to be constant over time, $\partial\overline{E}/\partial t=0$, and energy will only dissipate through bottom friction and interactions with vegetation. If this is the case, the change in wave energy flux in the direction of wave propagation can be expressed as

$$\frac{\partial\overline{F}}{\partial x}=-D_V-D_B \tag{14}$$

where D_V is the energy dissipated per unit area due to the interaction with the vegetation (N/ms) and D_B is the energy dissipated per unit area due to bottom friction (N/ms).

In dense vegetation stands, the energy loss caused by vegetation is usually larger than the energy loss caused by the bottom.

4.1 Wave energy dissipation due to vegetation

In many studies concerning wave damping by vegetation, the submerged parts have been treated as rigid vertical cylinders. The wave force acting on each vegetation element can then be calculated in the same way as for a pile on a costal structure. The horizontal fluid force acting on the submerged part of the cylinder is the sum of the inertia force and the drag force.

The force acting on a cylinder per unit length, f, (N/m) is (SPM, 1984)

$$f = f_i + f_D = C_m \frac{\pi D^2}{4} \frac{du}{dt} + C_d \frac{1}{2} \rho D u |u| \tag{15}$$

where f_i is the inertia force per unit length (*N/m*), f_D is the drag force per unit length (*N/m*), C_m is the inertia coefficient (*dimensionless*), C_d is the drag coefficient (*dimensionless*), D is cylinder diameter (*m*) and u is the horizontal water velocity at the axis of the cylinder.

In equation 15, it is assumed that the force per unit length, f, is dependent only on horizontal forces and not on vertical forces. According to Kobayashi et al. (1993) this assumption is acceptable.

The total force acting on a cylinder can only be calculated if the horizontal water velocity and acceleration are known at all depths. Linear wave theory can describe the depth dependence of both the water velocity and acceleration, but it can not account for the changes in the flow field caused by the cylinder.

The time average dissipation of energy due to the drag force acting on a cylinder per unit length, d_{dsc}, (*N/s*) is

$$d_{dsc} = u f_D = C_d \frac{1}{2} \rho D u^2 |u| \tag{16}$$

The drag coefficient of an object is determined by Reynolds number, the surface roughness, the objects shape and orientation in the flow field. Reynolds number is dependent on the wave induced water particle velocity, which declines with depth. This variation of Reynolds number with depth is not accounted for and the drag coefficient is assumed to be constant over the full depth. Reynolds number, Re, (*dimensionless*) is given by

$$\mathrm{Re} = \frac{u_{\max} D}{\nu} \tag{17}$$

where u_{max} is the peak water particle velocity at the still water level (*m/s*).

The time average energy loss of a wave due to the drag force acting on a single cylinder can be calculated, if equation 16 is time average integrated over a wave period and over the full depth.

$$\overline{D}_{dsc} = \left(\frac{1}{T}\right) \int_t^{t+T} \int_{-d}^{\eta} d_{dsc} \, dz dt = \frac{C_d \rho D}{2T} \int_t^{t+T} \int_{-d}^{\eta} |u|^3 \, dz dt \tag{18}$$

where $\overline{D}_{dsc}$ is the time average dissipated energy due to the drag force acting on a single cylinder (*Nm/s*) and η is the water surface elevation (*m*).

After substitution of equation 6 in equation18, it is seen that the phase angle, $\theta = (2\pi x/L - 2\pi t/L)$, is the only part of the orbital velocity which is time dependent. Where

x is the location of the cylinder and it is preferably set to zero. After substitution, equation 18 is first time average integrated over a wave period. This gives the time average dissipated energy per unit length of the cylinder due to the drag force, $\overline{d}_{dsc}$, (*Nm/s*) and it can be expressed as

$$\begin{aligned}\overline{d}_{dsc} &= \frac{C_d \rho D}{2T}\left(\frac{h}{2}\frac{gT}{L}\frac{\cosh\left[2\pi(z+d)/L\right]}{\cosh(2\pi d/L)}\right)^3 dz\int_0^T\left|\cos\left(-\frac{2\pi t}{T}\right)\right|^3 dt \\ &= \frac{2C_d \rho D}{3\pi}\left(\frac{h}{2}\frac{gT}{L}\frac{\cosh\left[2\pi(z+d)/L\right]}{\cosh(2\pi d/L)}\right)^3 dz\end{aligned} \tag{19}$$

To find the total drag induced energy loss of a wave when passing a cylinder equation 19 must be integrated over the full depth. Vegetation does usually not have cylindrical shape and constant diameter at all depths. To account for this it can be necessary to give the diameter of the cylinder some depth dependence. Reed does however have a quite uniform shape and diameter and it can therefore be regarded as a cylinder with constant diameter.

Equation 19 is now integrated from the lake bottom to the still water level to get the total energy loss of a wave caused by the drag force acting on a single cylinder.

$$\begin{aligned}\overline{D}_{dsc} &= \frac{2C_d \rho D}{3\pi}\left(\frac{h}{2}\frac{gT}{L}\right)^3\left(\frac{1}{\cosh(2\pi d/L)}\right)^3\int_{-d}^{0}\left(\cosh\left[2\pi(z+d)/L\right]\right)^3 dz \\ &= \frac{2C_d \rho D}{3\pi}\left(\frac{h}{2}\frac{gT}{L}\right)^3\left(\frac{1}{\cosh(2\pi d/L)}\right)^3\cdot \\ &\quad\left(\frac{1}{3}\frac{\sinh(2\pi d/L)\left(\cosh(2\pi d/L)^2+2\right)}{(2\pi/L)}\right)\end{aligned} \tag{20}$$

Equation 20 can be rewritten as

$$\overline{D}_{dsc} = \frac{2}{3\pi}C_d \rho D h^3\left(\frac{gk}{2\sigma}\right)^3\left(\frac{\sinh(kd)\left(\cosh(kd)^2+2\right)}{3k\cosh(kd)^3}\right) \tag{21}$$

where k is $2\pi/L$ (*1/m*) and σ *is* $2\pi/T$ (*1/s*).

The energy loss per unit area caused by the drag force can be calculated, if the reed density is known. The reed density is expressed as, N_c, the number of cylinders per unit area ($1/m^2$). The time average dissipation of energy per unit area caused by the drag force acting on an array of cylinders, $\overline{D}_{dac}$, (*N/ms*) can then be expressed as

$$\overline{D}_{dac} = \frac{2}{3\pi}C_d \rho N_c D h^3\left(\frac{gk}{2\sigma}\right)^3\left(\frac{\sinh(kd)\left(\cosh(kd)^2+2\right)}{3k\cosh(kd)^3}\right) \tag{22}$$

The inertia force acting on a vertical cylinder depends on the horizontal water particle acceleration. According to linear wave theory the horizontal water particle acceleration depends on the phase angle, $\theta = (2\pi x/L - 2\pi t/T)$. The time dependence of the phase angle causes the inertia force to cancel out over time, if the waves are periodic and symmetric. Waves in nature are however not perfectly periodic and symmetric. This discrepancy between linear wave theory and waves in nature should be kept in mind, when linear wave linear wave theory is applied on natural occurring waves. According to Dalrymple et al. (1984), the inertia force can be neglected, when the energy dissipation is induced by plants.

The wave energy dissipation caused by vegetation can, if neglecting the inertia force, be expressed as

$$D_v = D_{dac} = \frac{2}{3\pi} C_d \rho N_c D h^3 \left(\frac{gk}{2\sigma} \right)^3 \left(\frac{\sinh(kd)\left(\cosh(kd)^2 + 2\right)}{3k \cosh(kd)^3} \right) \tag{23}$$

Equation 23 is the same equation as the one presented by Dalrymple et al. (1984). Swaying motions of the plant is ignored in this model, but it can be correlated for by adjustments of the drag coefficient (Dalrymple et al., 1984).

4.2 Wave energy dissipation due to bottom friction

Wave energy dissipation due to bottom friction occurs if the wave orbitals reach down to the bottom. According to linear wave theory this is the case when the water depth is less than half the wave length. In dense vegetation stands, wave energy dissipation caused by vegetation is generally much larger than the wave energy dissipation caused by bottom friction. Bottom friction is therefore usually assumed to be negligible when vegetation is present. Bottom friction will however be considered in this study if a wave energy loss is observed for waves propagating through a control area without vegetation.

The wave energy dissipation due to bottom friction over smooth, rigid and impermeable bottoms can be divided into a laminar boundary layer case and turbulent boundary layer case. In nature, boundary layers are more frequently turbulent than laminar (Dean and Dalrymple, 1991). The boundary layers in the field study are however assumed to be laminar and according to Dean and Dalrymple (1991) boundary layers are laminar for smooth bottoms if Reynolds number is less than 10000. Reynolds number, R_b, (*dimensionless*) is given by

$$R_b = \frac{u_b \xi_b}{v} \tag{24}$$

where u_b is the peak horizontal velocity just above the boundary layer (*m/s*), ξ_b is maximum horizontal water particle excursion just above the boundary layer (*m*) and v is the viscosity (m^2/s).

Boundary layers under waves are thin. Those from linear wave theory predicted water motions at the bottom can therefore be assumed to be of the same size as the water motions just above the boundary layer. The peak horizontal velocity and the maximum horizontal water particle excursion just above the boundary layer are then given by the following equations.

$$u_b = \frac{h}{2}\frac{gT}{L}\frac{1}{\cosh(2\pi d / L)} \tag{25}$$

$$\xi_b = \frac{hgT^2}{4\pi L}\frac{1}{\cosh(2\pi d / L)} \tag{26}$$

The wave energy dissipation over impermeable, rigid and smooth bottoms with laminar boundary layers is given by (Dean and Dalrymple, 1991)

$$D_B = \frac{\nu k g h^2 \rho}{8\sinh(2kd)}\sqrt{\frac{\sigma}{2\nu}} \tag{27}$$

4.3 Resuspension due to waves

If water movements at the sediment surface induce a sufficiently high bed shear stress, resuspension can occur. Waves can generate water movements at the sediment surface if the water is shallower than half the wave length (SPM, 1984). These wave induced water motions are constantly changing direction and the peak bed shear stress will occur when the horizontal velocity just above the boundary layer is at its highest. The highest horizontal velocity just above the boundary layer will be referred to as the peak velocity. Since the peak velocity is easy to estimate from linear wave theory, it would be useful to find the peak velocity that coincides with the onset of sediment motion. The lowest peak velocity that can generate sediment motion will be referred to as the critical velocity.

The bed shear stress is caused by hydrodynamic forces acting on the bottom. The bed shear stress (equation 28) is the sum of:

- The skin friction (N/m^2), τ_s, which is the friction per unit area caused by the sediment particles.
- The form drag (N/m^2), τ_f, which is the pressure drag per unit area caused by ripples and other large variations in the bottom profile.
- The sediment transport (N/m^2), τ_t, which is the force per unit area required to bring sediment particles in motion.

$$\tau_0 = \tau_s + \tau_f + \tau_t \tag{28}$$

where τ_0 is the bed shear stress (N/m^2).

The peak skin friction caused by waves can be calculated by (Soulsby, 1997)

$$\tau_{ws} = \frac{1}{2} \cdot \rho \cdot f_w \cdot u_b^2 \tag{29}$$

where τ_{ws} is the peak skin friction caused by waves (N/m^2), f_w is the wave friction factor (*dimensionless*) and u_b is the peak velocity (m/s).

The peak velocity just above the boundary layer is given by equation 25. The wave friction factor is dependent on Reynolds number and the bottom roughness. For smooth bottoms with laminar boundary layers, the wave friction factor is given by (Soulsby, 1997)

$$f_w = \left(\frac{2}{\sqrt{R_b}} \right) \tag{30}$$

If the bottom is flat, no ripples exist and the sediment transport is small, then the skin friction almost equals to the bed shear stress. Equation 29 can under such conditions be used to calculate the peak bed shear stress caused by waves. For non-cohesive sediments Shields parameter can be used to calculate the critical bed shear stress (equation 31). According to Soulsby (1997), shields parameter can not only be used for steady currents, but also for oscillatory waves.

$$\tau_{cr} = \theta_{cr} \cdot g \cdot d_g \cdot (\rho_s - \rho) \tag{31}$$

where τ_{cr} is the critical bed shear stress (N/m^2), θ_{cr} is shields parameter (*dimensionless*), d_g is the grain diameter (m) and ρ_s is the density of the sediment (kg/m^3).

Shields parameter for non-cohesive sediments, can be estimated from (Soulsby, 1997)

$$\theta_{cr} = \frac{0.3}{1 + 1.2 \cdot D_*} + 0.055 \cdot \left(1 - e^{0.02 \cdot D_*}\right) \tag{32}$$

where D_* is the dimensionless grain size which is given by (Soulsby, 1997)

$$D_* = d_g \cdot \left(\frac{g \cdot ((\rho_s / \rho) - 1)}{\nu^2} \right)^{1/3} \tag{33}$$

If the peak skin friction is equal to the critical bed shear stress at the onset of sediment motion, the critical velocity can be estimated by combining equation 29 with equations 31 and 32.

$$u_{bcr} = \sqrt{\frac{\left(\frac{0.3}{1+1.2 \cdot D_*} + 0.055 \cdot \left(1 - e^{0.02 \cdot D_*}\right)\right) \cdot 2 \cdot g \cdot d_g \cdot (\rho_s - \rho)}{\rho \cdot f_w}} \tag{34}$$

where u_{bcr} is the critical orbital velocity just above the boundary layer (*m/s*).

It must be noted that equation 34 is restricted to non-cohesive sediments, horizontal and flat bottoms. Generally, sediment particles are lifted from the bottom into the water column when the peak velocity is significantly higher than the critical velocity.

5 Field study

The field measurements were conducted over a three week period in July 2006 at three sites in Lake Krankesjön. The sites were chosen because they had one or more characteristics that might influence the waves. It was assumed that results from one site alone or in a combination with the results from one or two of the other sites could be used to 1) study the effects on waves as they propagate through a stand of reed, 2) find site and initial wave characteristics of non or great importance to wave alterations within the reed stand and 3) evaluate the models presented in Chapter 4.

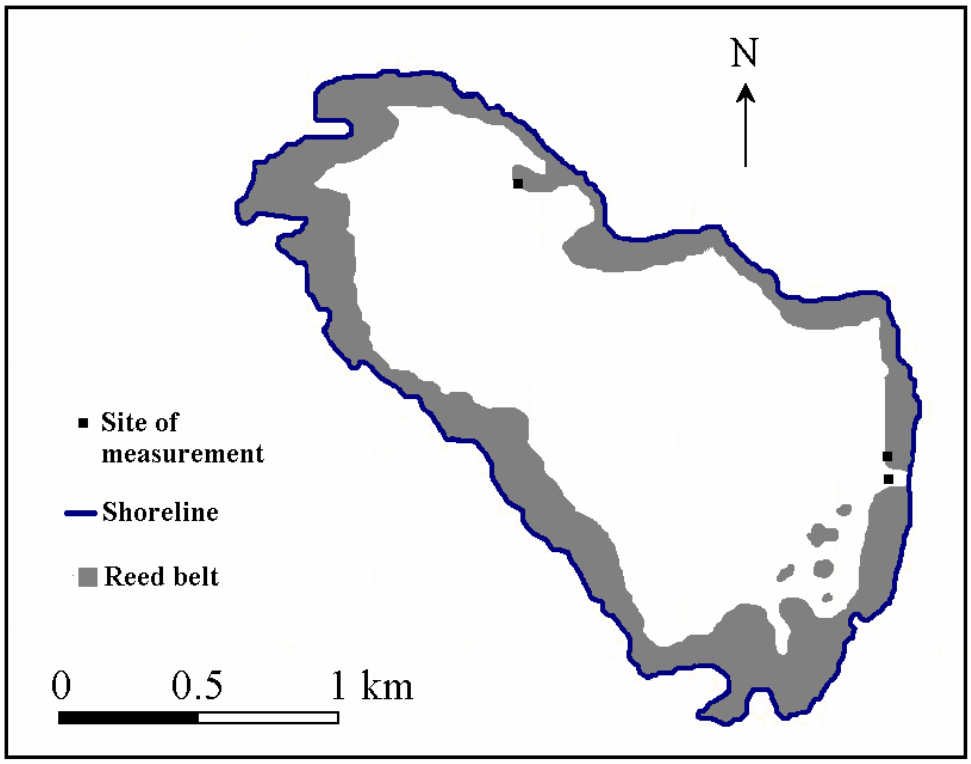

Figure 5. Map over Lake Krankesjön 2006. (Made by Charlotta Borell Lövstedt and edited by the author)

The sites of measurement can be seen in figure 5 and they will hereafter from north to south be referred to as, the deep water site, the shallow water site and the beach. A detailed description of each site is given in Chapter 5.2.

5.1 Field measurements

5.1.1 Wave measurements

Wave measurements were made along a transect perpendicular to the reed stands outer edge at the shallow and deep water site. Wave measurements at the beach were made along a transect in line with the direction of wave propagation. Six poles were placed along the transects and the distance between each pole were one to two meter. The poles will from outermost to the innermost pole be referred to as pole 1,2,3,4,5, and 6.

Two wave gauges were used in the test set up and they recorded the water surface displacement simultaneously over a three minute period. The three minute recording period was followed by seven minutes of no recording. These seven minutes were used to move one of the wave gauges. One of the wave gauges was attached to pole 1, the outermost, to record incoming waves. This wave gauge remained fixed to pole 1 and this wave gauge will hereafter be referred to as the fixed station. A second wave gauge was moved between the other poles placed along the transect. This wave gauge will be referred to as the movable station. It was initially attached to pole 2. The movable station was after each recording moved one pole away from pole 1. This was done until pole 6 was reached. At this pole two consecutive recordings were made. The movable station was then moved one pole per recording towards pole 1. This was done until pole 1 was reached. The whole procedure explained above will be referred to as a measurement cycle.

Each wave gauge has a float that moves up and down a vertical metal rod (Figure 6) and the water surface elevation is determined by the floats position on the rod. The wave gauge is connected to a data logger and an electrical signal is linearly correlated to the position of the float on the rod. The position of the float was recorded eight to ten times per second. In order to reduce the impact of the pole on the wave recordings the float was orientated towards the incoming waves. The distance between the pole and the float was approximately 10 cm.

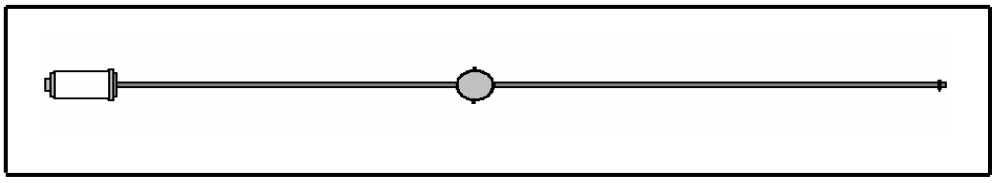

Figure 6. Wave gauge (laying down)

A boat was used at the field measurements and it was anchored on the leeward side of transect in order to reduce the impact of the boat on the wave recordings.

5.1.2 Abiotic measurements

To be able to compare measurement cycles, the incident wave angel was estimated. This was done at the beginning of each measurement cycle. The water depth was measured at all poles in order to evaluate the bottom's effect on waves. Depth measurements were made before the first measurement cycle was initiated at the site. Wind directions and wind speeds were measured before or under each measurement cycle. Wind measurements were made approximately 1.5 meter above the water surface with a hand held wind gauge. Since the wave gauge records the position of the float it is crucial to the reliability of the wave recording, that the float and the water surface are on level with each other. Generally, the float was on level with the water surface. However, a small fraction of the largest waves did have wave crests that passed slightly above the float. This difference between float elevation and surface elevation will be referred to as overtopping and if overtopping was observed, then a note was made. Notes about wave breaking were also made.

5.1.3 Reed measurements

Since it could be assumed that the reed it self is a main factor controlling wave alterations within reed stands, stem diameters and stem densities were measured. The stem diameter was measured at the still water level with a slide calliper. The stem density was measured at the still water level with a, $0.5m \cdot 0.5m$, square frame. This was done in order to map the density and extension of the reed stand. Different mapping techniques were applied at the sites and these techniques will be described in detail in chapter 5.2.1 and 5.2.3.

5.2 Site descriptions

Site specific measurement techniques and results from all measurements but wave measurements are presented in this Chapter.

5.2.1 The deep water site

All measurements were made from a boat at the deep water site. The effect of the boat on the measurements was believed to be negligible for all measurements except reed density measurements. The mapping of the reed stand was affected by the boat due to manoeuvring difficulties within the reed stand. The reed density was therefore approximated for large areas. These approximations were based on reed density measurements along the transect and the stands outer edge. The reed stand can be described as a monoculture of common reed and a rough map of its density and extension can be seen in figure 7. The first pole within the reed stand was pole 3 and it was situated approxemateley $0.5m$ from the edge of the reed stand. The average stem diameter was $8.4mm$.

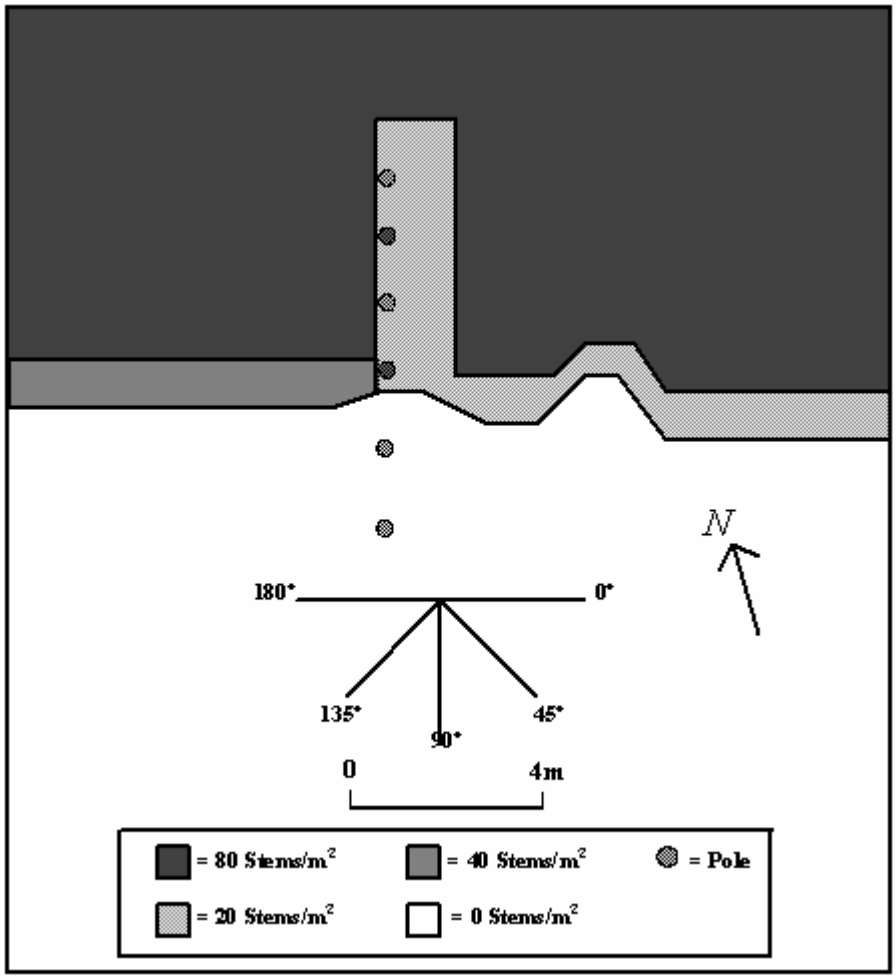

Figure 7. Map over the deep water site

The depths at the poles as well as the poles' distance from pole 1 are given in table 1.

Table 1. The water depth at the poles and the poles' distance from pole 1.

	Pole 1	Pole 2	Pole 3	Pole 4	Pole 5	Pole 6
Depth (*m*)	1.37	1.37	1.25	1.25	1.25	1.20
Distance from pole 1 (*m*)	0	2.17	4.14	5.64	7.30	8.96

Five measurement cycles were recorded and they will in chronological order be referred to as measurement cycle 1,2,3,4 and 5 at the deep water site.

Time, date, wind speed, wind direction and incident wave angel for the measurement cycles are given in table 2. Notes about wave breaking and overtopping are also found in table 2.

Table 2. Date, time, observed wind and wave characteristics for the measurement cycles at the deep water site.

	Measurement cycle 1	**Measurement cycle 2**	**Measurement cycle 3**	**Measurement cycle 4**	**Measurement cycle 5**
Date	060704	060705	060705	060706	060706
Time	11:07-12:40	11:47-13:20	16:07-17:40	11:47-13:20	15:47-17:20
Wind speed (*m/s*)	1.5-3	3-4.5	4-6	4-6	1.5-3
Wind direction	SSE	SE	SE	ESE	SSE
Incident wave angel (°)	35	30	20	30	40
Over-topping	No	No	Yes at pole 1,2 and 3	Yes at pole 1,2 and 3	No
Wave breaking	No	No	No	No	No

5.2.2 The beach

Vegetation was not present at this site and the wave measurements were made along a transect in line with the direction of wave propagation.

One measurement cycle was started, but it was brought to an end after pole 6 was reached. This measurement cycle will be referred to as measurement cycle 1 at the beach even though it is not complete. A complete measurement cycle was also recorded (hereafter: measurement cycle 2 at the beach). The poles were removed after each measurement cycle. The depth at the poles will therefore vary between the measurement cycles (table 3). The distance between one pole and the next was however kept constant at one meter.

In order to facilitate comparison with the shallow water site, the transects were placed so that the depth profile along the transects resembled the depth profile along transect at the shallow water site. This was done as far as it was possible.

Table 3. The water depth at the poles for measurement cycle 1 and 2 at the beach.

	Pole 1	Pole 2	Pole 3	Pole 4	Pole 5	Pole 6
Depth for measurement cycle 1 (*m*)	0.44	0.43	0.39	0.37	0.33	0.30
Depth for measurement cycle 2 (*m*)	0.45	0.45	0.45	0.43	0.42	0.42

Time, date, wind speed, wind direction for the measurement cycles are given in table 4. Notes about wave over topping and wave breaking are also given in table 4.

Table 4. Date, time, observed wind and wave characteristics for the measurement cycles at the beach.

	Measurement cycle 1	Measurement cycle 2
Date	060714	060718
Time	12:17-13:00	14:27-16:00
Wind speed (*m/s*)	5-8	6-9
Wind direction	NNW	NW
Overtopping	Yes	Yes
	at all poles	at all poles
Wave breaking	No	Yes
		at all poles but not very much

No bottom ripples were observed. A sediment sample was taken in order to make resuspension analysis possible. The sediment sample was sieved and the grain fractions found are given in figure 8. The sediment is non cohesive, because it is clastic and almost all grains are larger than 0.06mm.

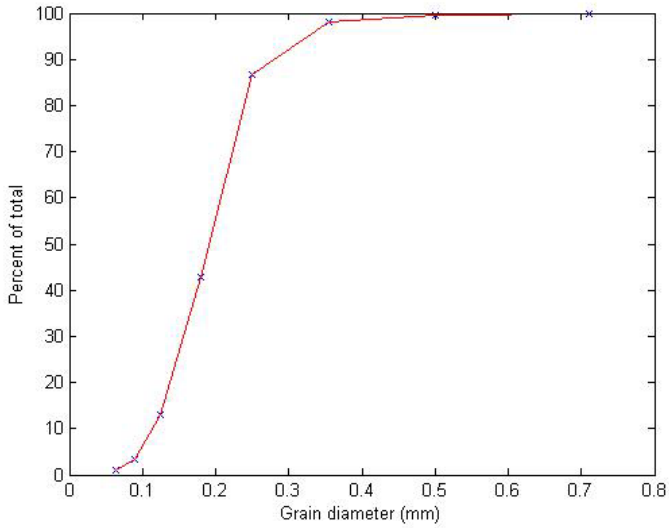

Figure 8. Weight percent of the sediment sample that is below a given grain diameter (*mm*).

5.2.3 The shallow water site

The water depth at the shallow water site made wading possible. As wading was possible the boat was no longer an obstacle to stem density measurements within the reed stand. To be able to make an accurate map over the reed stand, the poles along the transect were used as orientation points. The stem density was measured in lines perpendicular to the transect. An average of each line was then calculated. The stem density as well as the poles distances from the edge of the reed stand can be seen in figure 9. All measurements apart from stem density measurements were made from a boat.

The reed stand can be described as a monoculture of common reed and the average stem diameter was 4.1*mm*. Uprooted submerged macrophytes were found within the reed stand. It was assumed that the uprooted submerged macrophytes might affect the wave measurement and they were therefore removed as much as possible. This was done before each measurement cycle.

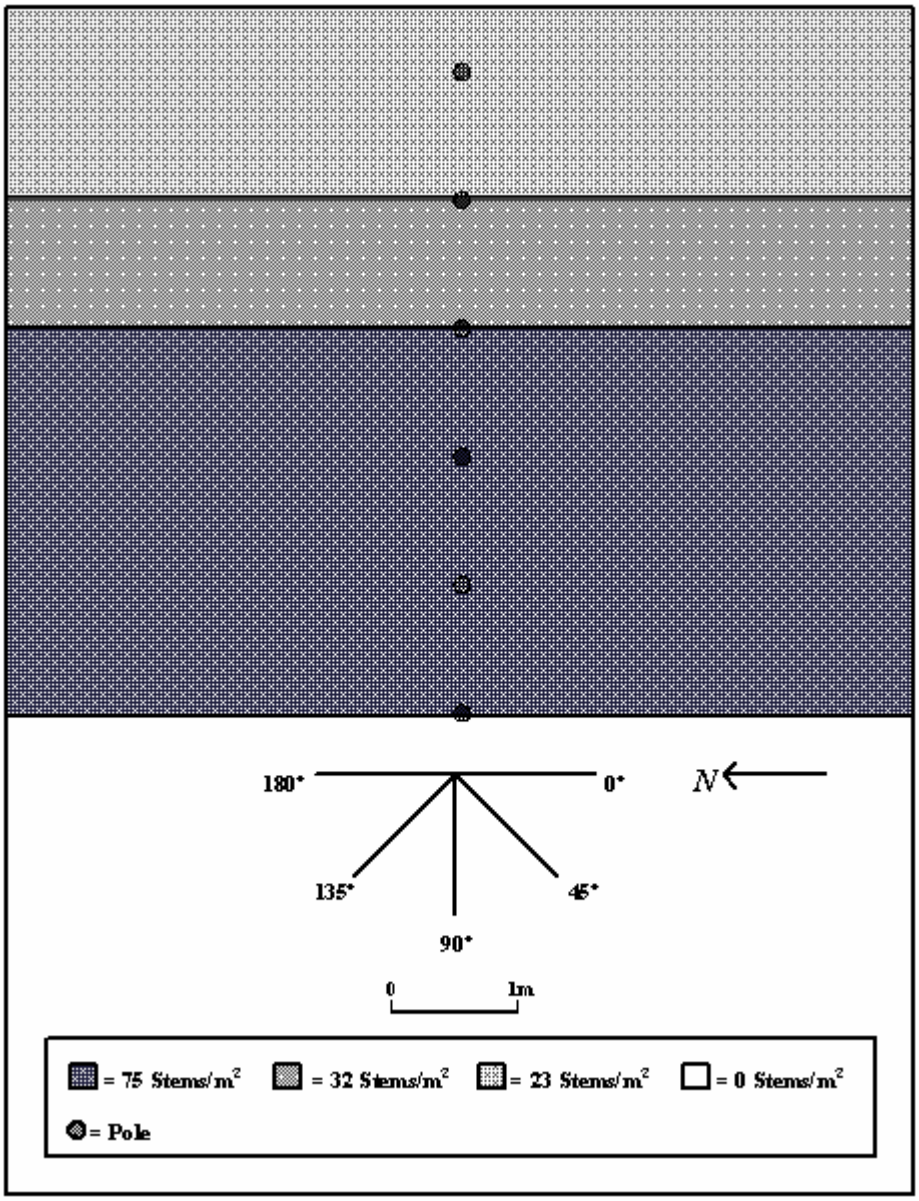

Figure 9. Map over the shallow water site

The distance from one pole to the next was one meter and the depth at each pole is given in table 5.

Table 5. The water depth at the poles.

	Pole 1	Pole 2	Pole 3	Pole 4	Pole 5	Pole 6
Depth (*m*)	0.45	0.43	0.42	0.40	0.38	0.36

Three measurement cycles were recorded and they will be referred to as measurement cycle 1,2 and 3 at the shallow water site. Time, date, wind speed, wind direction and incident wave angels for the measurement cycles are given in table 6. Notes about overtopping and wave breaking are also given in table 6.

Table 6. Date, time, observed wind and wave characteristics for the test cycles at the shallow water site.

	Measurement cycle 1	**Measurement Cycle 2**	**Measurement cycle 3**
Date	060714	060718	060718
Time	10:37 -12:10	12:47-14:20	16:07-17:40
Wind speed (*m/s*)	6-8	6-9	7-10
Wind direction	NNW	NW	NW
Incident wave angel (°)	110	110	110
Overtopping	Yes	Yes	Yes
	at pole 1 and 2	at pole 1 and 2	at pole 1,2 and 3
Wave breaking	No	No	No

No bottom ripples were observed and the sediment is assumed to resemble that of the beach.

6 Data analysis

The wave recordings in this study provide information on how the water surface elevation varies with time. To be able to study wave alterations it is necessary to have a strict definition of a wave. This definition can then be used to divide the wave recordings into small segments, where each segment contains information about a single wave. The zero-downcrossing method can be used to separate individual waves from a wave recording. A single wave is according to the zero-down crossing method initiated after a downward crossing of the still water level by the water surface and the wave is terminated by the next downward crossing of the still water level by the water surface (figure 10).

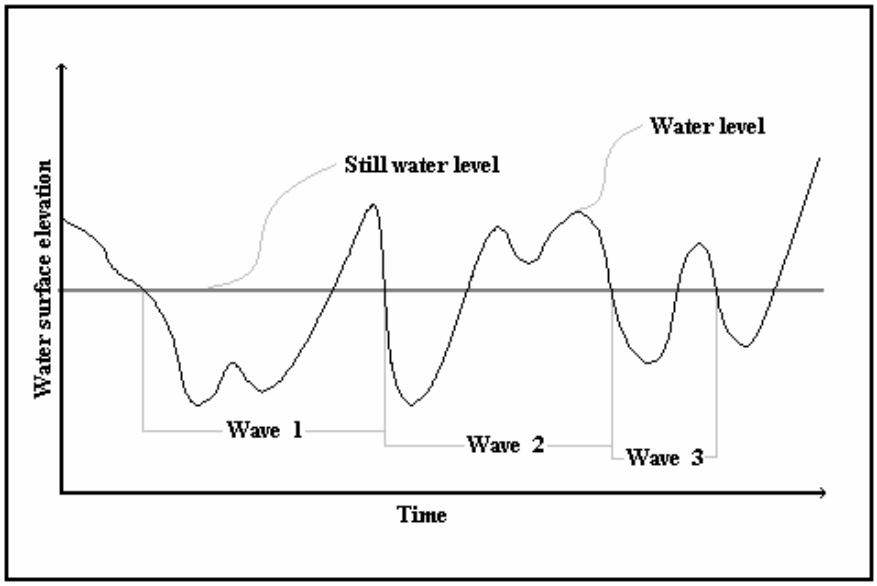

Figure 10. Individual waves within a wave recording according to the zero-downcrossing method

The wave period is according to the zero-downcrossing method defined as the time span between two consecutive crossings of the still water level by the water surface in a downward direction. This time span is termed the zero-downcrossing period and it indicates the beginning and end of a single wave. The wave height is according to the zero-downcrossing method defined as the difference between the highest and the lowest water surface elevation during a zero-downcrossing period. This wave height is called the zero-downcrossing wave height.

The frequency of occurrence of the zero-downcrossing wave heights within a deep water wave record are usually close to the frequency of occurrence given by the Rayleigh distribution. The Rayleigh distribution can therefore be used to compensate for small errors of measurement. These errors of measurement might be caused by overtopping and recording difficulties of the smallest wave heights.

Since single waves within a wave record have a wide range of wave heights and periods, it is desirable to find a representative wave that could be assumed to be statistically representative of all waves within the wave record. The average wave height of the one-third highest waves predicted from the Rayleigh distribution (hereafter: The significant wave height) and the average zero-down crossing period (hereafter: average period) are not only related to all waves within the wave record, they are also easy to calculate. The significant wave height and the average period will therefore be used to describe the representative wave.

The significant wave height is for a Rayleigh distributed wave spectrum given by (SPM 1984)

$$H = H_{rms}\sqrt{2} \tag{35}$$

where H is the significant wave height (m) and H_{rms} is the root mean-square wave height (m).

The root mean square wave height is given by (SPM 1984)

$$H_{rms} = \left(\frac{1}{N} \cdot \sum_{J=1}^{N} h_j^2 \right)^{1/2} \tag{36}$$

where N is the total number of waves within a wave record (*dimensionless*).

In this study it is assumed that the significant wave height and the average period along the reed stands outer edge are of roughly the same magnitudes as the significant wave height and the average period recorded at the fixed station. This assumption makes it possible to estimate the reed stands effect on a representative wave, even if the direction of wave propagation is not in line with the transect. The distance along the wave path from the stands outer edge to the movable station, is the distance of wave propagation in reed stand. The distance of wave propagation can be estimated from the site map if it is combined with the incident wave angel.

7 Wave attenuation models and critical orbital velocities

7.1 Wave attenuation models

Each study site has its set of characteristics. These characteristics affect the choice of wave attenuation model and the variables within the model. The wave attenuation model and the variables used for each site are given in this chapter.

The initial wave height and the initial wave period are in the wave attenuation models represented by the significant wave height and the average period at fixed station. The significant wave height and the average period are calculated for each recording period of three minutes. If these two variables and the water depth are known at the fixed station, then linear wave theory can be used to estimate the water motions and the wave energy density of the representative wave. The representative wave is assumed to be statistically representative of all waves that pass the fixed station over a three minute recording period. The wave attenuation models presented here predict the alteration of the wave energy density of the representative wave along its wave path. The wave energy density of the representative wave obtained from the model at a point of interest can be expressed as the significant wave height at that point.

The wave attenuation models applied are solved numerically.

7.1.1 The wave attenuation model at the deep water site

The deep water makes it possible to omit bottom friction and shoaling from the wave attenuation model at the deep water site. The wave attenuation model is therefore given by

$$\frac{\partial \overline{E}}{\partial x} = -\frac{\left(\frac{2}{3\pi} C_d \rho N_c D \left(\frac{8\overline{E}}{g\rho}\right)^{3/2} \left(\frac{gk}{2\sigma}\right)^3 \left(\frac{\sinh(kd)\left(\cosh(kd)^2+2\right)}{3k\cosh(kd)^3}\right)\right)}{C_g} \tag{37}$$

where x in this case is the distance of wave propagation within the reed stand (m).

Due to the mapping difficulties of the reed stand, a constant reed density of 56 stems per square meter is used. All non-wave related parameters in equation 37 are given in table 7.

Table 7. Non-wave related parameters used in the wave attenuation model at the deep water site

N_c *(dimensionless)*	*D (mm)*	*ρ (kg/m³)*	*g (m/s²)*
56	*8.4*	1000	9.81

The drag coefficient is used to adjust the wave attenuation model to the reed stand and the prevailing wave condition.

7.1.2 The wave attenuation model at the beach

Wave energy dissipation caused by vegetation is not included in wave attenuation model at the beach, since no vegetation is present. The wave attenuation model is therefore given by

$$\frac{\partial \overline{E}}{\partial x} = -\frac{\left(\frac{vk\overline{E}}{\sinh(2kd)}\sqrt{\frac{\sigma}{2v}}\right)}{C_g} \tag{38}$$

where x in this case is the distance of wave propagation from pole 1 (m)

The bottom topography is assumed to change stepwise (table 8) in the wave attenuation model and the bottom contours are assumed to be perpendicular to the transect.

Table 8. Bottom topography along the transect at the beach.

	Distance from Pole 1 0-0.5 (m)	Distance from Pole 1 0.5-1.5 (m)	Distance from Pole 1 1.5-2.5 (m)	Distance from Pole 1 2.5-3.5 (m)	Distance from Pole 1 3.5-4.5 (m)	Distance from Pole 1 4.5-5 (m)
Depth for measurement cycle 1 (*m*)	0.44	0.43	0.39	0.37	0.33	0.30
Depth for measurement cycle 2 (*m*)	0.45	0.45	0.45	0.43	0.42	0.42

In the wave attenuation model the wave energy flux just before a step in the bottom topography is assumed to be equal to the wave energy flux just after the step. Equation 12 is therefore used in the wave attenuation model to calculate the shoaling at the step.

All non-wave related parameters in equation 38 are given in table 9.

Table 9. Non-wave related parameters used in the wave attenuation model at the beach.

v (m^2/s)	*ρ* (kg/m^3)	*g* (m/s^2)
$1.005 \cdot 10^{-6}$	1000	9.81

Some relevant objections can be raised against the use of the bottom friction model when evaluating the wave attenuation at the beach and the shallow water site. The smoothness of the bottom might be disturbed by roots, rhizomes and reed stems. The bottom is probably permeable, but to a very limited extent. The bottom is not rigid, but it is in this case better described as rigid than viscous. Even though objections can be made, the model might provide useful information on the relative size of the wave energy dissipation caused by bottom friction.

7.1.3 The wave attenuation model at the shallow water site

The choice of wave attenuation model at the shallow water site depends on the bottom friction. Bottom friction will be included in the wave attenuation model (equation 39), if the wave attenuation model at the beach make good predictions or if it underestimates the wave attenuation. Otherwise bottom friction will be omitted from the wave attenuation model (equation 40).

$$\frac{\partial \overline{E}}{\partial x} = -\frac{\left(\frac{2}{3\pi} C_d \rho N_c D \left(\frac{8\overline{E}}{g\rho}\right)^{3/2} \left(\frac{gk}{2\sigma}\right)^3 \left(\frac{\sinh(kd)\left(\cosh(kd)^2+2\right)}{3k\cosh(kd)^3}\right)\right)}{C_g} - \frac{\left(\frac{vk\overline{E}}{\sinh(2kd)}\sqrt{\frac{\sigma}{2v}}\right)}{C_g} \tag{39}$$

$$\frac{\partial \overline{E}}{\partial x} = -\frac{\left(\frac{2}{3\pi} C_d \rho N_c D \left(\frac{8\overline{E}}{g\rho}\right)^{3/2} \left(\frac{gk}{2\sigma}\right)^3 \left(\frac{\sinh(kd)\left(\cosh(kd)^2+2\right)}{3k\cosh(kd)^3}\right)\right)}{C_g} \tag{40}$$

where x in these case are the distance of wave propagation within the reed stand (m).

The bottom topography is assumed to change step wise (table 10) in the two wave attenuation models and the bottom contours are assumed to be perpendicular to the transect.

Table 10. Bottom topography along the transect at the shallow water site.

	Distance from Pole 10-0.5 (m)	Distance from Pole 1 0.5-1.5 (m)	Distance from Pole 1 1.5-2.5 (m)	Distance from Pole 1 2.5-3.5 (m)	Distance from Pole 1 3.5-4.5 (m)	Distance from Pole 1 4.5-5 (m)
Depth (*m*)	0.45	0.43	0.42	0.40	0.38	0.36

Shoaling is included in the two wave attenuation models and it is calculated in the same way as it was for the wave attenuation model at the beach. The reed density

used in the applied model is given by figure 9. All other non-wave related parameters used in equation 39 or 40 are given in table 11.

Table 11. Non-wave related parameters used in the wave attenuation model at the shallow water site.

v (m^2/s)	ρ (kg/m^3)	g (m/s^2)	D (mm)
$1.005 \cdot 10^{-6}$	1000	9.81	4.1

7.2 Critical orbital velocities

The critical orbital velocities are estimated with equation 34 for the beach and the shallow water site. The grain diameter that is used to calculate the critical orbital velocity is the diameter of grains at the fifty cumulative weight percent point, d_{50}. d_{50} is 0.190 *mm* for the sediment sample at the beach. The density of the grains is assumed to be as that of quarts, 2650 kg/m^3. The viscosity and the density of water are, respectively, 1.005 m^2/s and 1000 kg/m^3.

8 Results

The results presented in chapter 8.1.1 to 8.1.3 and 8.2.1 to 8.2.3 are based on the average of the two wave recording periods at a given pole within a measurement cycle. If only one recording is obtained for a given pole within a measurement cycle, then this single recording is used to calculate variables and ratios related to that specific pole.

A battery failure occurred when the movable station was attached to pole three for the first time in measurement cycle 1 at the shallow water site. The float on the movable station got tangled up in the reed when the movable station was attached to pole six in measurement cycle 2 at the shallow water site. This did also occur when the movable station was attached to pole four for the second time in measurement cycle 1 at the deep water site. These recordings will therefore not be used in this study.

8.1 Results from wave measurements

Generally, the wave heights within a wave record were close to being Rayleigh distributed. However, small variations between wave regimes with high and low wave heights were observed. The largest wave heights within wave records with a high wave regime were usually lower than the wave heights expected from the Rayleigh distribution (figure 11 and 12). The largest wave heights within wave records with a low wave regime were on the other hand usually close to being Rayleigh distributed (figure 13). The deviation from the Rayleigh distribution of the largest recorded wave heights, was however quite constant for all three minute wave records within a measurement cycle, exemplified by figure 11B and 12B.

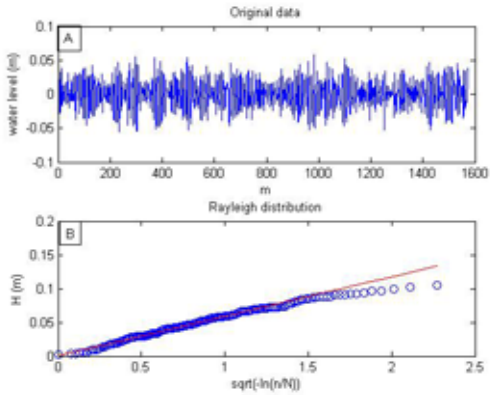

Figure 11A. The water surface displacement over time at the fixed station, when the movable station is mounted to pole 6 for the second time in measurement cycle 2 at shallow water site. The time is here given by m which is the number of recordings of the water surface elevation within the recording period.

Figure 11B. Rayleigh and observed wave height distribution at the fixed station, when the movable station is mounted to pole 6 for the second time in measurement cycle 2 at the shallow water site. N is the total number of waves. n is the rank of a wave. Waves within a wave record are here ranked by wave height from the highest to the lowest.

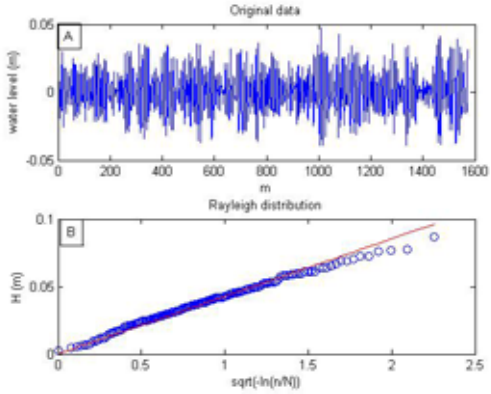

Figure 12A. The water surface displacement over time at the movable station, when it is mounted to pole 6 for the second time in measurement cycle 2 at shallow water site. The time is here given by m which is the number of recordings of the water surface elevation within the recording period.

Figure 12B. Rayleigh and observed wave height distribution at the movable station, when the movable station is mounted to pole 6 for the second time in measurement cycle 2 at the shallow water site. N is the total number of waves and n is the rank of a wave. Waves within a wave record are here ranked by wave height from the highest to the lowest.

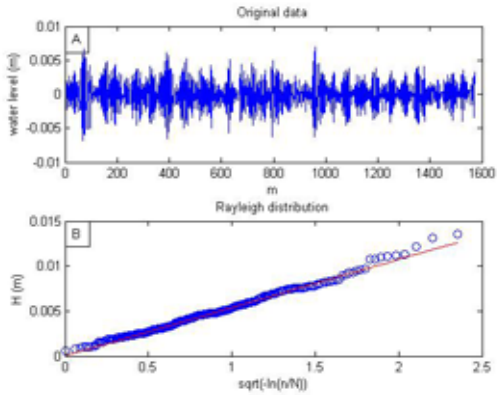

Figure 13A. The water surface displacement over time at the movable station, when it is mounted to pole 6 for the second time in measurement cycle 1 at deep water site. The time is here given by m which is the number of recordings of the water surface elevation within the recording period.

Figure 13B. Rayleigh and observed wave height distribution at the movable station, when the movable station is mounted to pole 6 for the second time in measurement cycle 1 at the deep water site. N is the total number of waves and n is the rank of a wave. Waves within a wave record are here ranked by wave height from the highest to the lowest.

The periods and wave heights varied within each recording period of three minutes (figure 11A, 12A, 13A). The significant wave heights and the average periods at the fixed station varied within each single measurement cycle (exemplified by figure 14A and B).

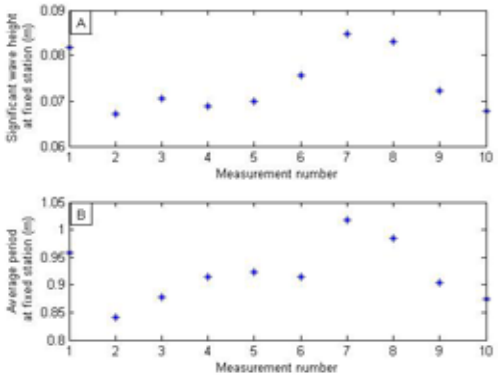

Figure 14A. The significant wave height at the fixed station for each individual wave recording in measurement cycle 3 at the deep water site.

Figure 14B. The average period at the fixed station for each individual wave recording in measurement cycle 3 at the deep water site.

Visual characterization of waves within and just outside the reed stand was made and it was observed that:

- Small wind generated ripples existed on top of the main waves outside the reed stand, when the wind was strong enough to generate them.

- Small wind generated ripples did not occur on top of the main waves within the reed stand

8.1.1 Results from wave measurements at the deep water site

A quite wide range of wave regimes were recorded at the deep water site and the significant wave heights at the fixed station can be seen in figure 15. All significant wave heights and average periods recorded at the deep water site are given in appendix 1.

Figure 15 shows that the decrease in the significant wave height per meter reed varies between 0.5 and 6.5 percent and that the decrease is not dependent on the significant wave height.

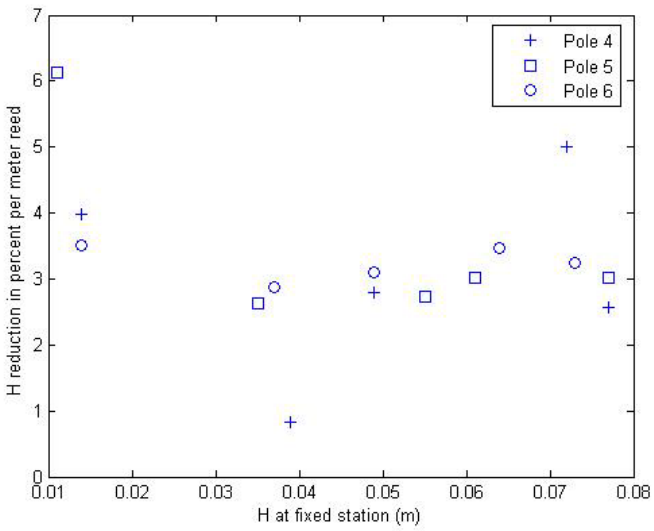

Figure 15. The relationship between the significant wave height reduction in percent per meter reed at pole 4, 5 and 6 and the significant wave height at the fixed station – at the deep water site.

Figure 16 shows that the significant wave height ratio between the movable and the fixed station tend to decreases with the distance of wave propagation in the reed stand.

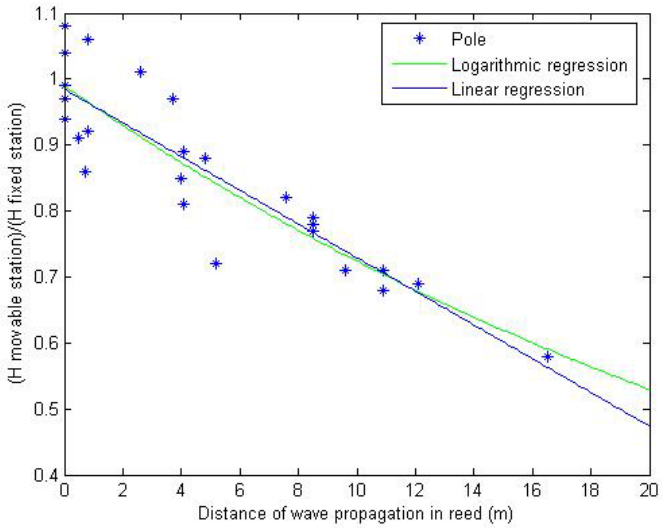

Figure 16. The relationship between the damping of the significant wave height and the distance of wave propagation in reed – at the deep water site.

The linear regression line is given by $y = 0.984 - 0.0255x$ and the R^2 value is 0.81.The logarithmic regression line is given by $ln\ y = -0.0105-0.0313x$ or $y = 0.990 \cdot 0.969^x$ and the R^2 value is 0.83. The significant wave height reduction per meter reed is according to the logarithmic regression 3.1 percent, which is close to the average wave damping per meter reed at pole 4, 5 and 6 (see figure 15). The significant wave height reduction per meter reed is according to the linear regression 2.6 percent of the initial wave height per meter reed.

The significant wave height ratio between pole 1 and 2 range from 0.94 to 1.08.

Figure 17 shows that the average period of waves with small significant wave heights are more strongly affected by the reed stand than the average period of waves with large significant wave heights.

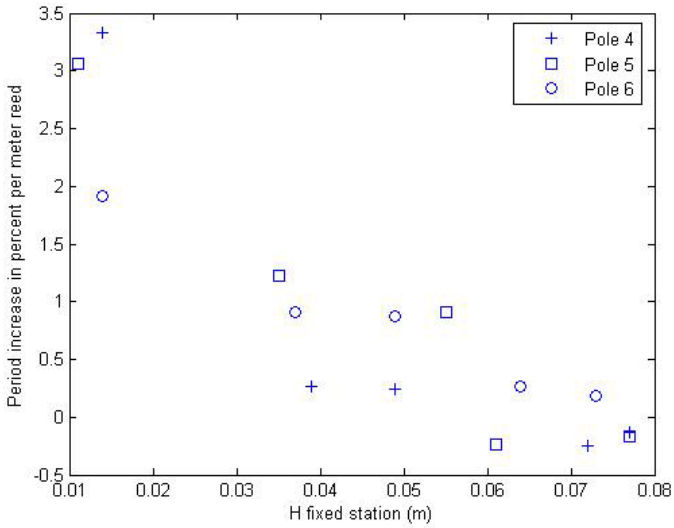

Figure 17. The relationship between the average period increase in percent per meter reed at pole 4, 5 and 6 and the significant wave height at the fixed station –at the deep water site.

The average period ratio between pole 1 and 2 range from 0.97 to 1.03.

8.1.2 Results from wave measurements at the beach

A quite narrow range of high wave conditions were recorded at the beach and the significant wave heights at the fixed station can be seen in figure 19. All significant wave heights and average periods recorded at the beach are given in appendix 2.
The significant wave heights are generally larger at the fixed station than at the movable station (figure 18). The decrease in significant wave height is generally larger for measurement cycle 2 than for measurement cycle 1.

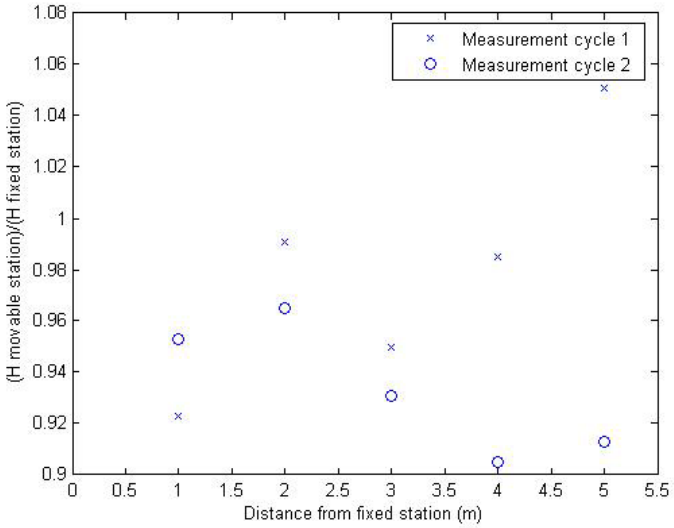

Figure 18. The relationship between the damping of the significant wave height for measurement cycle 1 and 2 and the distance of wave propagation from the fixed station –at the beach.

The average period increase per meter is plus minus two percent (figure 19).

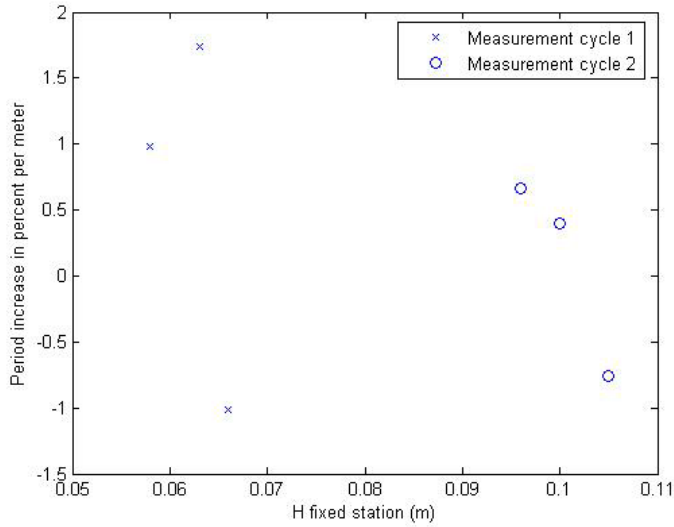

Figure 19. The relationship between the average period increase in percent per meter for measurement cycle 1 and 2 and the significant wave height at the fixed station –at the beach.

The estimated ranges of Reynolds number, and the ranges of the peak and critical orbital velocities between pole 2 and 6 are given for each measurement cycle in table 12.

Table 12. The range of Reynolds number, and the ranges of the peak and critical orbital velocities within each measurement cycle at the beach.

	Measurement cycle 1	Measurement cycle 2
The range of Reynolds number (Dimensionless)	400-1500	1600-2700
The range of the Peak velocity (*m/s*)	0.06-0.1	0.1-0.12
The range of the critical orbital velocity (*m/s*)	0.05-0.07	0.07-0.08

8.1.3 Results from wave measurements at the shallow water site

A narrow range of relatively high wave regimes were recorded at shallow water site and the significant wave heights at the fixed station are given in figure 20.The recorded significant wave heights and average periods are given in appendix 3.

Figure 20 shows that significant wave height reduction is three to seven percent per meter reed and the decrease seems to be independent of the significant wave height. The average reduction of the significant wave height is roughly 5 percent per meter reed.

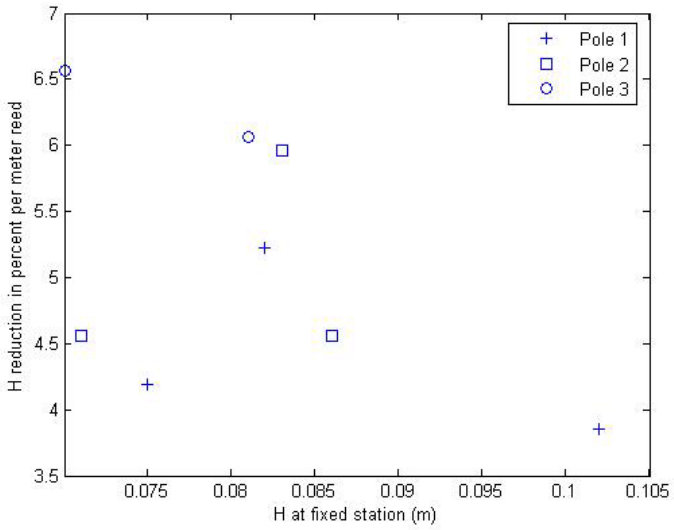

Figure 20. The relationship between the significant wave height reduction in percent per meter reed at pole 4, 5 and 6 and the significant wave height at the fixed station – at the shallow water site.

Figure 21 shows that the ratio between the significant wave height at the movable station and significant wave height at the fixed station tend to decreases with the distance of wave propagation in the reed stand.

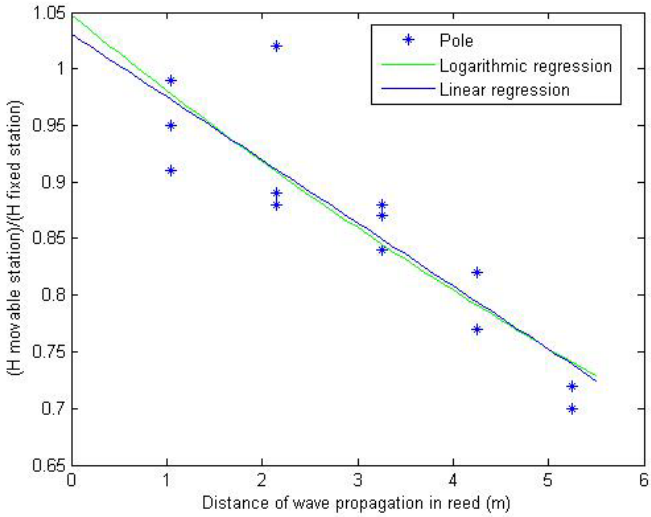

Figure 21. The relationship between the damping of the significant wave height and the distance of wave propagation in reed – at the shallow water site.

The linear regression line is given by $y = 1.03 - 0.056x$ and the R^2 value is 0.79.The logarithmic regression line is given by $ln\ y = 0.047\text{-}0.066x$ or $y = 1.05 \cdot 0.94^x$ and the R^2 value is 0.80.

The significant wave height reduction per meter reed is according to the logarithmic regression 6 percent, which is slightly higher than the average wave damping per meter reed at pole 4, 5 and 6 (see figure 20).

Figure 22 shows that the average period usually is larger within the reed stand than outside.

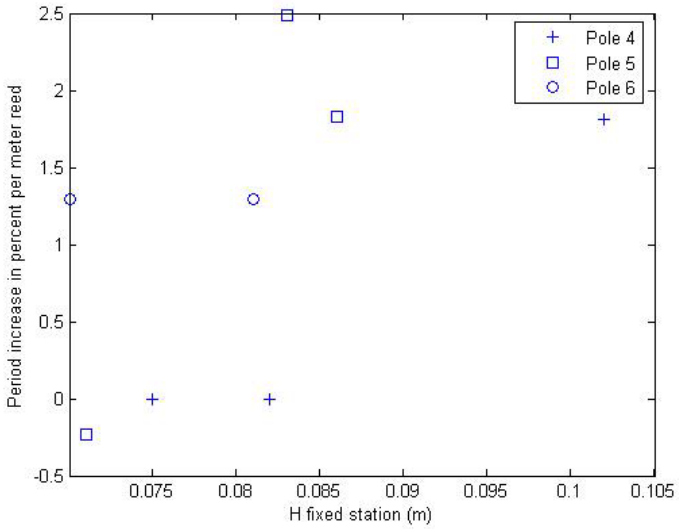

Figure 22. The relationship between the average period increase in percent per meter reed at pole 4, 5 and 6 and the average period at the fixed station – at the shallow water site.

The ranges of Reynolds number at the bottom, and the ranges of the peak and critical orbital velocities between pole 2 and 6 within each measurement cycle are given in table 13.

Table 13. The range of Reynolds number, and the ranges of the peak and critical orbital velocities within each measurement cycle at the shallow water site.

	Measurement cycle 1	Measurement cycle 2	Measurement cycle 3
The Range of Reynolds number (*Dimensionless*)	500-1600	700-1600	2100-3500
The Range of the peak velocity (*m/s*)	0.06-0.09	0.08-0.09	0.11-0.14
The range of the critical orbital velocity (*m/s*)	0.05-0.07	0.06-0.07	0.07-0.08

8.2 Results from the wave attenuation models

Since drag coefficients are known to vary with Reynolds number, it is necessary to find out if a relationship exists between Reynolds number and the drag coefficients applied in the models.

Figure 23 shows how the drag coefficient varies with Reynolds number. The drag coefficients presented in this graph are the ones that generate perfect agreement in the

significant wave height damping between the applied model and a three minute recording period.

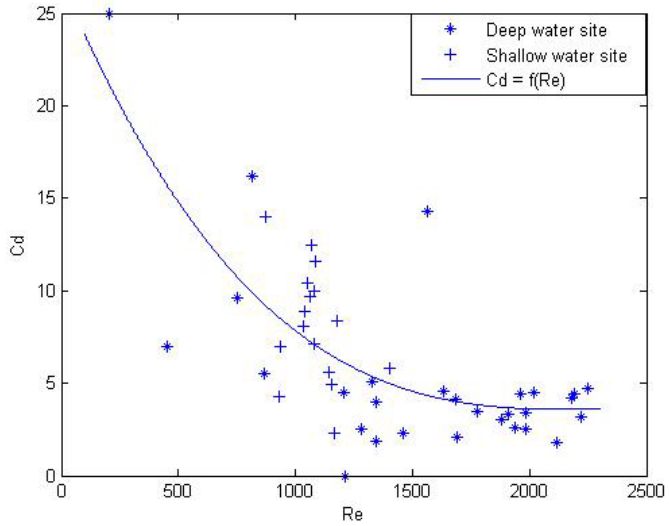

Figure 23. Drag coefficients versus Reynolds number and the drag coefficient as function of Reynolds number.

The line in figure 23 represents the drag coefficient as a function of Reynolds number. This function is given by $C_d = 26.7 - 0.0296 \cdot Re + 1.26 \cdot 10^{-5} \cdot Re^2 - 1.75 \cdot 10^{-9} \cdot Re^3$ and it is obtained through a least square interpolation. The interpolation is based on all data points given in figure 23. Because the drag coefficient function is empirical and of third order it should only be used within the observed range of Reynolds number, 200-2300.

The results obtained from the wave attenuation models are hereafter based on Hm/H0 ratios. Where H0 is the significant wave height at the fixed station and Hm is the significant wave height at movable station, which is obtained from the model or from the wave measurement. The graphs in this chapter are equipped with a reference line called the line of perfect fit and it represents a perfect agreement between modelled and recorded Hm/H0 ratios.

The drag coefficient used in the applied wave attenuation model at the shallow and the deep water site is either given by the function of Reynolds number or by the average of all perfect fit drag coefficients used in that specific model. The perfect fit drag coefficient is the drag coefficient that generates a perfect agreement in the Hm/H0 ratio between the model and the three minute recording period. A perfect fit drag coefficient can be obtained from the applied model for all three minute recording periods at the shallow and deep water site, if the damping of the significant wave height occurs. For individual wave measurements with increasing significant wave heights, the perfect fit drag coefficient is set to zero.

8.2.1 Results from the wave attenuation model at the deep water site

Figure 24 shows the agreement between measured and modelled Hm/H0 ratios when the average of all perfect fit drag coefficients is used in the model. This average is 5.32. This model underestimates the damping of the significant wave heights for waves with Re<1200, while it mostly overestimates the damping of the significant wave heights for waves with Re>1200 (figure 24).

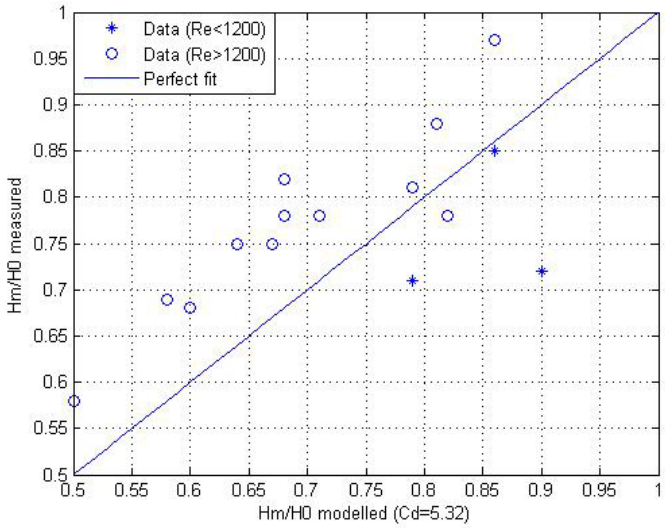

Figure 24. Comparison between measured and modelled H/H0 ratios at the deep water site -the average drag coefficient is used in the model.

Figure 25 shows the agreement between measured and modelled Hm/H0 ratios when the drag coefficient is given as a function of Reynolds number. The drag coefficient used ranges from 4 to 24 (figure 23). The agreement between modelled Hm/H0 ratios is quite good for waves with Re<1200 and waves with Re>1200 (figure 25).

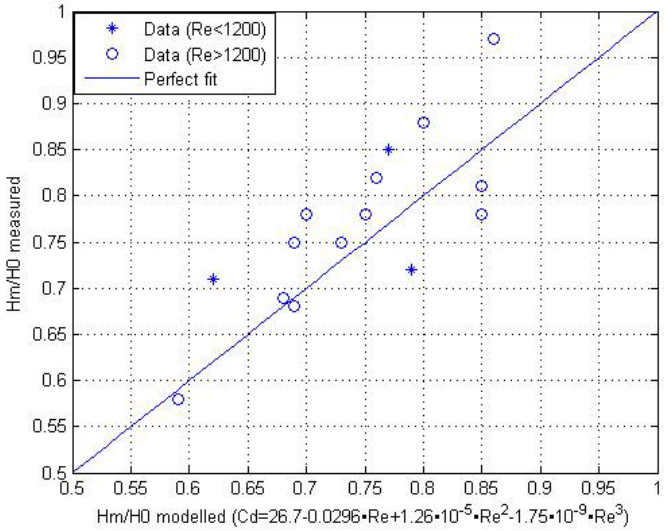

Figure 25. Comparison between measured and modelled H/H0 ratios at the deep water site - the drag coefficient function is used in the model.

8.2.2 Results from the wave attenuation model at the beach

Figure 26 shows a very low agreement between modelled and measured Hm/H0 ratios. The model underestimates the damping of the significant wave heights for measurement cycle two, while it both under- and overestimates the damping of the significant wave heights for measurement cycle one.

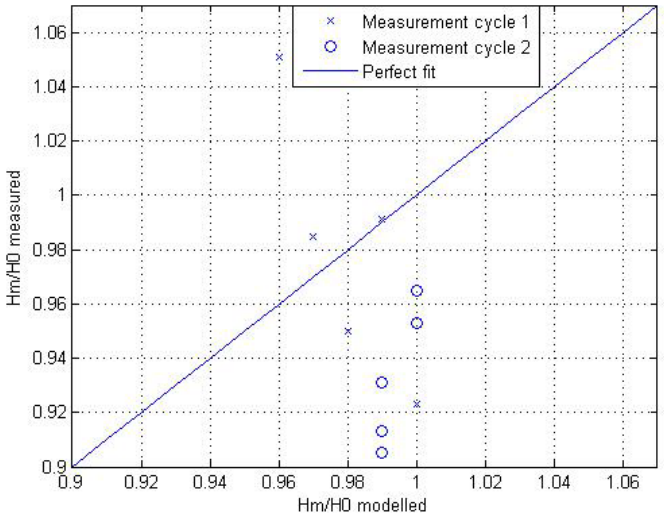

Figure 26. Comparison between measured and modelled H/H0 ratios at the beach.

8.2.3 Results from the wave attenuation model at the shallow water site

Since the wave attenuation model at the beach underestimates the damping of the significant wave height in most cases, bottom friction will be included in the wave attenuation model at the shallow water site. Equation 39 is therefore used to model the wave attenuation at the shallow water site.

Figure 27 shows the agreement between modelled and measured Hm/H0 ratios when the average of all perfect fit drag coefficients is used in the model. This average is 8.16. The variation in modelled of Hm/H0 ratios is smaller than the variations in measured Hm/H0 ratios (figure 27).

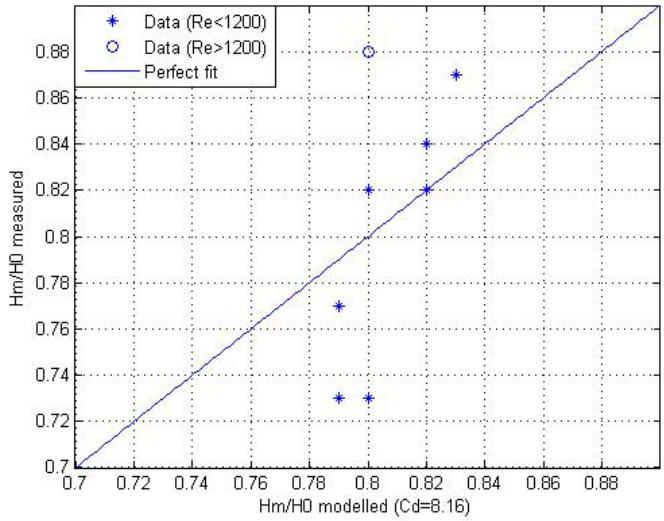

Figure 27. Comparison between measured and modelled H/H0 ratios at the shallow water site - the average drag coefficient is used in the model.

Figure 28 shows the agreement between measured and modelled Hm/H0 ratios when the drag coefficient is given as a function of Reynolds number. The drag coefficient used ranges from 5 to 11 (figure 23). The variation in modelled Hm/H0 ratios is smaller than the variation in measured Hm/H0 ratios (figure 28).

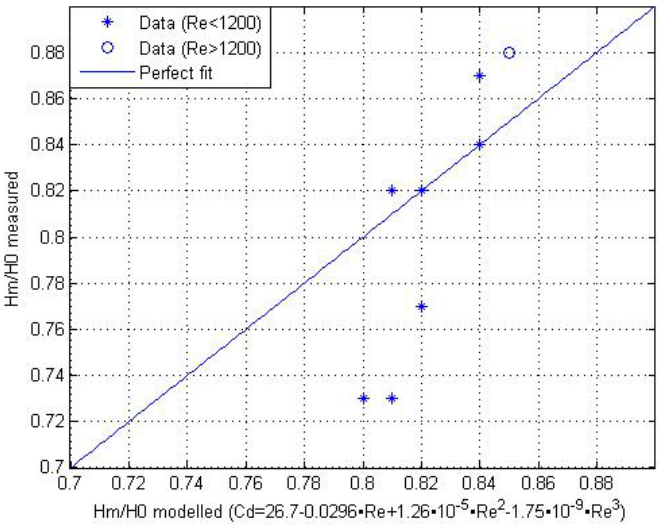

Figure 28. Comparison between measured and modelled H/H0 ratios at the shallow water site - the drag coefficient function is used in the model.

9. Discussion

The average damping of the significant wave heights per meter is approximately 3 percent at the deep water site and 5 percent at shallow water site. Based on these averages, a representative wave with an initial significant wave height of 12c*m* will have a significant wave height of approximately 9*cm* after travelling 10*m* in the reed stand at the deep water site, while it will have a wave height of approximately 7c*m* after travelling 10*m* in the reed stand at the shallow water site.

The agreement between the modelled and measured damping at the deep and the shallow water site is quite good when the drag coefficient is given as a function of Reynolds number.

9.1 Wave measurements

The small divergence between recorded wave heights and those expected from the Rayleigh distribution (figure 11B, 12B and 13B), indicates that the significant wave height expected from the Rayleigh distribution represents the average wave height of the one-third highest waves quite well. Observed divergences of this kind are similar for all wave recordings within a measurement cycle, compare figure 11B and 12B. The probability distribution of the frequency occurrence of H_{rms} scaled wave heights is therefore probably close to constant for all wave recordings within a measurement cycle. And since the probability distribution of the H_{rms} scaled wave heights is close to constant along the transect in the reed stand, then it is probably constant along the wave path in the reed stand too. The probability distribution of the H_{rms} scaled wave heights can only remain constant along the wave path in the reed stand, if all wave heights within the wave height spectra are attenuated equally much. This indicates that the reed induced damping of the wave height is independent of the initial wave height.

Variations in the significant wave height and average period within a measurement cycle (figure 14A and B) can be explained by variations in the wave regime during the measurement cycle, but also to some extent by the periodicity of small and large waves (figure 11A and 12A and 13A). If a wave recording starts at the beginning of a group of small waves and ends just after a group of small waves, then the recorded significant wave height will be lower than if it had started a few moments earlier. The periodicity of small and large waves can therefore be a source of error in the wave damping analysis.

Variations in the significant wave height and the average period were observed between two poles, pole 1 and 2, outside the reed stand at the deep water site. The largest observed difference between these two poles is 8 percent for the significant wave height (figure 16) and 3 percent for the average period. If differences like these are observed between pole 1 and 2 at the deep water site, then it can be assumed that differences in significant wave height and average period will occur between the reed stand's outer edge and the fixed station too. The difference in significant wave height and average period between the fixed pole and the reed stand's outer edge is a source of error in the wave damping analysis. The results from the wave measurements were

presented graphically in two ways. One way was to present the relationship between the alteration and the distance of wave propagation from a given point. The other way was to present the relationship between the alteration in percent per meter and the significant wave height at the fixed station.

For the results presented as the relationship between the alteration and a distance from the reed stand's outer edge is the source of error caused by variations in significant wave height or average period between the fixed pole and the reed stand's outer edge not altered along the wave path in the reed stand. It can be questioned if this is a source of error because the alteration is given as ratio between movable station and the fixed station. This alteration is however in this study interpreted as the alteration from the reed stands outer edge to the movable station.

For results presented as the relationship between the alteration in percent per meter reed and the significant wave height, is the source of error caused by variations in significant wave height or average period between the fixed pole and the reed stand's outer edge declining with the distance of wave propagation in the reed stand. If the significant wave height at the fixed pole is six percent lower than at the point of interest at the reed stand's outer edge, then the error in this wave damping analysis is roughly 12 percent if the distance of wave propagation is half a meter, while the error is only about one percent if the distance of wave propagation is six meter. For this reason the results obtained from pole 2 and 3 at the shallow and deep water site was not used in this kind of graphical presentation.

The applied wave analysis of the significant wave heights and the average periods does not account for variations in the reed density. Therefore, variations in the reed density can explain small variations in average periods and significant wave heights between poles. Small variations in the reed density have greater impact on the wave analysis for shorter distances than longer distances of wave propagation in reed, because variations like these tends to even out with distance.

9.1.1 The deep water site

The lowest recorded wave regimes might be sensitive to measurement errors related to the detection limit of the wave gauge.

The maximum hypothetical translocation of the fixed station is 16 meter. The initial source of error caused by the hypothetical translocation can be assumed to be the same size or even larger than the variation in significant wave height and average period observed between pole 1 and 2. If this, the mapping difficulties and the periodicity of small and large waves are kept in mind, then the damping of significant wave height by roughly three percent per meter reed seems quite consistent (figure 15).

The agreement between both the linear and the logarithmic regression line and the recorded significant wave heights are very good (figure 16). The logarithmic regression represents a damping in percent per meter, while linear regression represents a linear damping. At short distances of wave propagation the logarithmic and the linear regression lines are close to each other, but they do depart more and

more from each other as the distance of wave propagation in the reed increases. Since most of the wave recordings are made at distances of wave propagation in the reed where the two regression lines are very close to each other (figure 16), it is hard to tell which on of them that give the best representation of the significant wave height damping. Based on the results is it therefore impossible to say if the damping is linear or if the damping is in percent per meter. The linear damping does however not seem very plausible, because then the damping in percent per meter increases exponentially with the distance of wave propagation in reed.

The results indicate that the damping of the significant wave height is independent of the initial significant wave height (figure 15), while alteration of the average period is dependent on the initial significant wave height (figure17). Wave regimes with a low significant wave height have a larger number of waves with low wave heights than wave regimes with a high significant wave height. Therefore will a larger number of waves with low wave heights be damped by the reed to a level below the detection limit for low than for high initial significant wave heights. If waves within a wave record are undetected by the wave gauge or completely attenuated, then the observed average period increases. Consequently, the observed average period will increase more for wave records with low initial significant wave heights than for wave records with high initial significant wave heights.

9.1.2 The beach

Since the direction of wave propagation is in line with the transect at the beach, no hypothetical translocation of the fixed station is required. For this reason, no analysis error caused by the hypothetical translocation of the fixed station can occur. An unexplainable large damping of the significant wave heights are however observed between pole one and two (figure 18). This indicates that other sources of errors than that caused by the translocation exist. One such source of error might be overtopping, which was frequent at all poles at the beach due to the high wave regime and the low damping along the transect.

The results indicate that the significant wave height damping is more pronounced for measurement cycle 2 than for measurement cycle 1 (figure 18). This might be explained by the wave breaking that occurred in measurement cycle 2.

The average period seems to be quite unaffected along the transect (figure 19) and the observed variations in average period might be explained by natural variations.

Since the sediment is non-cohesive, no ripples exists on the bottom and the boundary is laminar, equation 34 can be used to calculate the critical orbital velocity. The peak velocities exceed the critical orbital velocity for all measurement cycles (table 12). This indicates that the d_{50} grains were brought into motion. The peak velocities are however not significantly higher than the critical orbital velocities, which indicate that d_{50} grains will remain on the bottom. Smaller sediment grain sizes might however go into suspension. That some resuspension occurred at the beach on the days of measurement can be supported by the high water turbidity.

9.1.3 The shallow water site

The maximum translocation of the fixed station is 2 meter and since pole 1 is located at the edge of the reed stand and pole 2 is located within the reed stand, it is hard to make a rough estimation of the source of error caused by the hypothetical translocation. The source of error caused by the hypothetical translocation at shallow water site can however be assumed to be of roughly the same size as that between pole 1 and 2 at the deep water site. The short distances of wave propagation in reed make analysis of wave alterations in percent per meter reed sensitive to sources of error caused by the hypothetical translocation. If this is kept in mind, then the damping of the significant wave height of roughly 5 percent per meter seems quite consistent (figure 20). The results indicate that the damping of the significant wave height is independent of the initial significant wave height.

Both the logarithmic and the linear regression line show good agreement with the observed significant wave heights (figure 21). The logarithmic regression represents a damping in percent per meter, while the linear regression represents a linear damping. The later damping does however not seem very plausible (see the discussion in chapter 9.1.1), but it gives a good approximation at short distances of wave propagation in reed.

The results indicate that the wave period increases in the reed stand (figure 22). The short distances of wave propagation can generate translocation errors, which are large in comparison with total alteration of the average period caused by the reed. This and the low number of wave recordings make it hard to tell by how much the average period is altered and if this alteration is dependent on the initial significant wave height.

Since the sediment is assumed to resemble that of the beach and the critical orbital velocities were exceeded by the peak velocities for all measurement cycles (table 13), it can be assumed that the d_{50} grains were brought into motion. The peak velocities were not significantly higher than the critical orbital velocities, which indicate that d_{50} grains will remain on the bottom. Smaller sediment particles might however be lifted into the water column.

9.1.4 Comparison of the sites

The significant wave height damping per meter reed at the shallow water site is roughly two percent larger than that at the deep water site (compare figure 15 and 20). The larger damping at the shallow water site can not be explained by a larger stem diameter or a higher reed density, because the average stem diameter at shallow water site is less than half of that at the deep water site and the reed density is of roughly the same at both sites. Bottom friction and shoaling (figure 18) on the other hand can explain why the damping is larger at the shallow than at the deep water site, but they can probably not explain the whole difference in significant wave height damping. For this reason, additional explanations must exist. It is likely that some of the uprooted submerged macrophytes that were tangled up in the reed at shallow water site were not removed. Remaining uprooted submerged macrophytes might explain some of the difference in significant wave height damping between the shallow and the deep water site. The difference in the significant wave height damping between

the shallow and the deep water site might also be explained by differences in the wave induced drag. This is discussed in chapter 9.2.

The difference in significant wave height damping between the shallow water site and the beach supports the idea that reed damp waves heights (compare figure 18 and 21). Since wave breaking was observed for measurement cycle 2 at the beach but not for measurement cycle 2 and 3 at the shallow water site, it can be assumed that reed stands reduce wave breaking. All these three measurement cycles are close to each other in time and the distance between the shallow water site and the beach is short.

A dependence between the initial significant wave height and the increase in average period was observed for waves propagating through the reed stand at the deep water site (figure 17), but not at the shallow water site (figure 22). This might be due to that only wave regimes with high initial significant wave heights were recorded at shallow water site, while both wave regimes with high and low significant wave heights were recorded at the deep water site. At the deep water site the average period increase per meter reed was large for wave regimes with low initial significant wave heights, while the average period increase per meter reed was close to zero for wave regimes with high initial significant wave heights.

9.2 Wave attenuation models

Since the perfect fit drag coefficient is adjusted in order to give the best agreement between the modelled and the measured Hm/H0 ratio, there is a risk that model errors not related to the drag coefficient is compensated for. One such source of error might be a low agreement between the reed density at the site and that applied in the model. Another source of error for the perfect fit drag coefficient is the error that might appear when the fixed pole is translocated.

The perfect fit drag coefficients are quite constant for Reynolds number 1200-2300 (figure 23). This indicates that the drag coefficient of reed is quite constant for Reynolds number larger than 1200. According to Finnemore and Franzini (1997), the drag coefficient of a circular cylinder is quite constant and roughly 1 for steady state conditions and Reynolds number 1000 to 10000. For steady state conditions and Reynolds number less than 1000 on the other hand, the drag coefficient of a circular cylinder increases with declining Reynolds number (Finnemore and Franzini, 1997). This can explain why the perfect fit drag coefficients increases drastically when Reynolds number becomes lower than 1200. Reynolds number 1200 seems critical to the drag coefficient of reed, and it coincides quit well with the critical Reynolds number of a circular cylinder. Large variations in the perfect fit drag coefficients exist below the critical Reynolds number of 1200 (figure 23). Kobayashi et al. (1993) plotted the drag coefficients of artificial kelp, i.e. plastic straps, against Reynolds number. The drag coefficients of artificial kelp and their corresponding Reynolds number where obtained from a wave tank experiment. The drag coefficients are quite constant for Reynolds number higher than 8000, while they tend to increase with decreasing Reynolds number when Reynolds number is less than 8000. Large variations in the drag coefficients of artificial kelp are observed for Reynolds number less than 8000. Reynolds number 8000 seems critical to the drag coefficient of artificial kelp. This critical Reynolds number of artificial kelp is much higher than

that observed for reed. This might not only be due to differences in shape between the two types of ”vegetation”. It might also be due to that swaying motions are larger for kelp than for reed. The similar and the strong influence on the observed drag coefficients below the critical Reynolds number for the two “vegetation” types indicates that the critical Reynolds number is important when evaluating the effect of vegetation on waves. It also indicates that it is hard to estimate the drag coefficient when the drag coefficient varies a lot with Reynolds number.

It can be assumed that variations in the reed density even out with distance. This is one of the reasons why only wave measurements obtained from pole 4, 5 and 6 are used in the analysis of the shallow and deep water attenuation model. An error caused by the hypothetical translocation of the fixed pole can be large when compared to the overall significant wave height damping caused by the reed. The quotient between this error and the overall significant wave height damping can be assumed to be larger at short distances than at long distances of wave propagation in reed. This is another reason why only wave measurements obtained from pole 4, 5 and 6 are used in the analysis of the shallow and deep water wave attenuation model.

Since the models can not compensate for an increase in the average period, they can not reflect the wave regime. The models can however be assumed to reflect the faith of a single wave, if the wave period of this single wave is constant along the wave path. The single wave used in the wave attenuation models is the representative wave at the fixed pole.

9.2.1 The wave attenuation model at the deep water site

The majority of the representative waves at the fixed station have a Reynolds number larger than 1200 and the perfect fit drag coefficients are quite constant for these representative waves. A few representative waves have a Reynolds number smaller than 1200 and the perfect fit drag coefficients for these representative waves are high with large variations.

When the average of the perfect fit drag coefficients is used in the model, the model underestimate the damping for representative waves with Reynolds number less than 1200, while it generally overestimate the damping for representative waves with Reynolds number larger than 1200 (figure 24). This overestimation of the damping by the model for representative waves with Reynolds number larger than 1200 is of a few percent and quite constant. This overestimation is caused by the high perfect fit drag coefficients of the representative waves with Reynolds number less than 1200. The constant overestimation with a few percent indicates that the model can predict the damping of the representative wave quit well, but that the applied drag coefficient is poorly chosen.

When the drag coefficient applied in the model is given as a function of Reynolds number, the model both under- and overestimates the damping of representative waves (figure 25). These under- and overestimations occur for both representative waves with Reynolds number above and below 1200. The agreement between modelled and measured Hm/H0 ratios is better when the drag coefficient is given by

the function of Reynolds number than when it is given by the average of the perfect fit drag coefficients (compare figure 24 and 25).

Some small variations between the modelled and the measured Hm/H0 ratios might be explained by translocation errors or by a low resemblance between the reed density applied in the model and that of the reed stand. In the model, the reed stand is assumed to be homogeneous with respect to reed density and stem diameter. The reed measurements indicate however that this is not case. Nevertheless, the model makes fairly good predictions of the damping of the representative waves. This indicates that variations in reed stand tend to even out along the wave path in the reed stand. The good model predictions can however not be used to verify that the correct reed density or stem diameter have been used in the model, because the drag coefficient applied in the model might compensate for such discrepancies. Based on the model alone, it is therefore not possible to tell if the applied drag coefficients actually represent that of reed.

9.2.2 The wave attenuation model at the beach

Since Reynolds number is smaller than 10^4 for both measurement cycles (table 12), the boundary layer can be assumed to be laminar if the bottom is smooth. The choice of bottom friction model seems therefore correct with respect to the boundary layer if the bottom is smooth. The bottom might however not be perfectly smooth.

The bottom friction model can not account for wave breaking and this might be one of the main reasons why the model underestimates the damping of the representative waves for measurement cycle 2 (figure 26). The agreement between modelled and recorded Hm/H0 ratios is not good for measurement cycle 1 (figure 26). This might be due to that the variation in significant wave heights along the transect is much larger than the damping.

The modelled damping of the representative waves is larger for measurement cycle 1 than 2 (figure 26) and this is due to that the modelled shoaling is more pronounced for measurement cycle 1 than 2 (compare the depth profiles in table 3).

9.2.3 The wave attenuation model at the shallow water site

Since the bottom friction model at the beach generally underestimates the damping of the representative wave, bottom friction is included in the wave attenuation model at shallow water site. It is however questionable if this underestimation is caused mainly by bottom friction or wave breaking. The inclusion of bottom friction in the shallow water model is therefore not obvious. The inclusion of bottom friction in the model will however not affect the model much, because the modelled damping of the representative waves are mainly caused the by the vegetational part of the model.

For representative waves with Reynolds number less than 1200, no major difference in the damping is observed for the two drag coefficients (figure 27 and 28). For the representative wave with a Reynolds number larger than 1200 on the other hand, the

model makes a better prediction of the damping of the representative wave when the drag coefficient is given as a function of Reynolds number than when it is given as an average of the perfect fit drag coefficients (compare figure 27 and 28).

The wave measurements indicate that the damping of the representative waves is quite constant in the reed stand (figure 21). The reed density applied in the model varies with the distance from the reed stands outer edge (the reed density applied in the model is given in figure 9). This affects modelled damping of the representative waves. The low reed density applied in the model between pole 3 and 6 can probably explain the narrow rage of damping expected from the models (figure 27 and 28).

9.2.4 Comparison of the site models

The average perfect fit drag coefficient for the shallow water model is approximately 1.5 times higher than the average perfect fit drag coefficient for the deep water model. One explanation might be that most of the representative waves at the shallow water site have a Reynolds number less than 1200, while the most of the representative waves at the deep water site have a Reynolds number greater than 1200. Another explanation might be might be that some uprooted submerged macrophytes were tangled up in the reed at the shallow water site.

The drag coefficients applied in the models ranged from 4 to 24 and seem therefore high when compared to that of a circular cylinder, 0.9-1.4, within the same range of Reynolds number. This might be explained by that reed have some subsurface leaves and that the reed densities used in the models are based on the reed density measurements. The reed density measurements were made at the water surface and they can therefore not account for all subsurface reed stems. A high abundance of old reed stems were visually observed below the water surface. The drag coefficient in the shallow and the deep water model is therefore adjusted in order to compensate for the subsurface reed stems. The drag coefficients applied in the models do therefore become higher than the true drag coefficient of reed.

The shallow and deep water model is tested but the validity of these two models are not truly evaluated, because the models were adjusted to the prevailing wave regimes with the drag coefficient. The drag coefficient seems however to be dependent on Reynolds number.

9.3 Common reed and its effect on resuspension and turbidity

The resuspension analysis at the beach indicates that sand grains, *190 μm*, within non-cohesive sediment are brought into motion, when the wind speed is *6-9m/s* and the water depth is 0.42-0.45*m*. The high turbidity observed on the days of measurement at the beach can be seen as indicator of resuspension. During these days the wind speed was 5-9*m/s*. Since the average water depth in Lake Krankesjön is 0.7*m*, the results and observations given above indicate that large areas within Lake Kranesjön might be affected by wave induced sediment motion and resuspension. Vegetation can however if present stabilize sediments through several mechanisms and thereby reducing sediment motion and resuspension.

When the two maps (figure 1 and 5) of Lake Krankesjön are compared it is seen that the reed stands had almost the same extension in 1981 as in 2006. This indicates that that extension of the reed stands have not changed very much for the past 25 years. Based on this it can be assumed that the stabilising effects of reed on sediments have been quite constant for the past 25 years.

The wave measurements support the idea that stands of common reed damp the significant wave height, which generates a decrease in the resuspension potential of waves. The observed increase in the average period within stands of common reed might on the other hand generate an increase in the resuspension potential of waves. The actual importance of the increase in average period to wave induced resuspension depends on which waves within the wave spectra that are affected. Within a wave regime that causes resuspension, waves with high wave heights and long wave periods contribute much more to the overall resuspension than waves with low wave heights and short wave periods. An increase in the average period can therefore affect the resuspension potential of a wave regime very much or very little. One extreme scenario is that the whole increase in the average period is caused by an increase in the wave length of the largest waves, which will generate a strong increase in the resuspension potential of the wave regime. The other extreme is that the whole increase in average period is caused by an increase in the period of the smallest waves, which will leave the resuspension potential of the wave regime unaffected. Since no analysis of individual wave periods are made, it is not possible to tell how much the increase in the average period affects the resuspension potential of the wave regime. Based on the analyses of the average periods and the significant wave heights, it is therefore not possible to verify or reject the idea that stands of common reed reduce wave induced resuspension.

The difference in wave breaking between measurement cycle 2 at the beach and measurement cycle 2 and 3 at the shallow water site (table 4 and 6) indicate that stands of common reed reduce wave breaking. Wave breaking is most pronounced in shallow areas at high wave regimes and it results in high water turbulence. This water turbulence can cause resuspension of sediments. Stands of reed can therefore at high wave regimes reduce sediment resuspension caused by breaking waves. This will in turn affect water turbidity. For lakes with extensive stands of reed in shallow areas, the reed stands effect on wave breaking might be an important factor controlling the water transparency at high wave regimes.

10 Conclusions

It has been seen that the significant wave height decreases along the wave path in the reed stands. The observed decreases in significant wave height were 0.5 to 7 percent per meter reed. Large variations in the damping of the significant wave height were observed between two stands of reed. This difference in damping was not possible to explain by variations in stem diameter or reed density, but maybe by uprooted vegetation that was tangled up the reed stands and variations in the wave induced drag.

It has been seen that the average wave period tend to increase along the wave path in the reed stand. The increase in average wave period seemed to be dependent on the initial significant wave height at one of the two reed stands studied. At the other reed stand no dependence was observed between the average wave period and the initial significant wave height, which might be due to that only a narrow range of wave regimes were recorded at this stand.

Based on the analyses of the significant wave heights and the average wave periods, it has not been possible to verify or reject the idea that stands of reed reduce the resuspension potential of wave regimes. This was due to the fact that no analysis of individual wave periods within a wave regime was made.

Based on the test of the shallow and the deep water model, the drag coefficient of reed seems to be rather constant for Reynolds Number larger 1200, while it seems to vary a lot for Reynolds number less than 1200.

A difference in wave breaking has been observed between a control area without reed and a reed stand next to it. Wave breaking occurred in the control area but not in the reed stand. This finding indicates that resuspension of sediments caused by breaking waves are reduced by reed stands.

11 Recommendations for further studies

The wave gauges could be calibrated in a wave tank, in order to evaluate the accuracy of the wave measurements and to find the wave detection limit of the wave gauges.

The wave analysis could be improved by a longer transect. This is due to idea that sources of errors related to the translocation of the fixed station and reed densities have less impact on the wave analysis at long than short distances of wave propagation. These sources of errors become small compared to the overall effect caused by reed at long distances.

To be able to make a true evaluation of the wave attenuation models for reed, it is essential to find the true range of drag coefficients. The range of drag coefficients of reed might be obtained from a wave tank experiment. The drag coefficient given as function of Reynolds number could however if combined with more wave measurements be used to evaluate the applicability of model on natural occurring common reed stands.

To be able to evaluate reed stands effect on the resuspension potential of wave regimes, it is necessary to analyse the reed stands effect on the wave periods of individual waves. The wave periods of individual waves must then be linked to their corresponding wave heights, in order to evaluate stands of reeds effect on the resuspension potential of wave regimes.

Wave measurements could be combined with resuspension measurement, in order to get even better under standing of waves effect on resuspension.

Turbidity data from lakes with various reed densities, but with great similarities in nutrient status, topography etc could be used to evaluate reed stands effect on turbidity.

12 References

Publications

Asano Toshiyuki, Deguchi Hiroshi, Kobayashi Nobuhisa. 1992. Interaction between water waves and vegetation. Proceedings of the Twenty-Third Coastal Engineering Conference, ASCE. 2710-2723.

Beglin T, Caffrey J M. 1996. Bank side stabilisation through reed transplantation in a newly constructed Irish canal habitat. Hydrobiologia 340. 349-354.

Blindow Irmgard, Hargeby Anders, Andersson Gunnar. 2002. Seasonal changes of mechanisms maintaining clear water in a shallow lake with abundant *Chara* vegetation. Aquatic Botany 72. 315-334.

Coops Hugo, Geilen Noël, Verheij Henk J, Boeters René, van der Velde Gerard. 1996. Interactions between waves, bank erosion and emergent vegetation: an experimental study in a wave tank. Aquatic Botany 53. 187-198.

Dalrymple Robert A, Kirby James T, Hwang Paul A. 1984. Wave diffraction due to areas of energy dissipation. Journal of Waterway, Port, Costal, and Ocean Engineering 110 (1). 67-79.

Dean Robert G, Bender Christopher J. 2006. Static wave setup with emphasis on damping effects by vegetation and bottom friction. Costal Engineering 53. 149-156.

Dean Robert G, Dalrymple Robert A. 1991. Water wave mechanics for engineers and scientists, Second printing. World Scientific Publishing Co. Singapore.

Finnemore John E, Franzini Joseph B. 1997. Fluid Mechanics with Engineering Applications, Ninth Edition. McGraw-Hill. Belfast.

Haslam S M. 1972. *Phragmites communis* Trin. The Journal of Ecology 60. 585-610.

Horppila Jukka, Nurminen Leena. 2001. The effect of an emergent macrophyte (*Thypha augustifolia*) on sediment resuspension in a shallow north temperate lake. Freshwater Biology 46. 1447-1455.

Hansson Lars-Anders, Annadotter Helene, Bergman Eva, Hamrin Stellan F, Jeppesen Erik, Kairesalo Timo, Luokkanen Eira, Nilsson Per Ake, Søndergaard Martin, Strand John. 1998. Biomanipulation as an Application of Food-Chain Theory: Constraints, Synthesis, and Recommendations for Temperate Lakes. Ecosystems 6 (1). 558-574.

Jönsson Anette, Danielsson Åsa, Rahm Lars. 2005. Bottom type distribution based on wave friction velocity in the Baltic Sea. Continental Shelf Research 25. 419-435.

Kobayashi Nobuhisa, Raichle Andrew W, Asano Toshiyuki. 1993. Wave attenuation by vegetation. Journal of Waterway, Port, Coastal, and Ocean Engineering 119 (1). 30-48.

Lantmäteriverket. 1993. Blå kartan, 31 Malmö, 3 edition. Lantmäteriverket. Gävle.

Luettich Richard A, Harleman Donald R F, Somlyody Laszlo. 1990. Dynamic behaviour of suspended sediment concentrations in shallow lake perturbed by episodic wind events. Limnology and Oceanography 35 (5). 1050-1067.

Massel S R, Furukawa K, Brinkman R M. 1999. Surface wave propagation in mangrove forests. Fluid Dynamics Research 24. 219-249.

Mendez Fernando J, Losada Inigo J. 2004. An empirical model to estimate the propagation of random and nonbreaking waves over vegetation fields. Coastal Engineering 51. 103-118.

Möller I. 2006. Quantifying saltmarsh vegetation and its effect on wave height dissipation: Results from a UK East coast saltmarsh. Estuarine, Costal and Shelf Science 69. 337-351.

Ostendorp Wolfgang, Iseli Christoph, Krauss Manfred, Krumscheid-Plankert Priska, Moret Jean-Louis, Rollier Maurice, Schanz Ferdinand. 1995. Lake Shore deterioration, reed management and bank restoration in some Central European lakes. Ecological Engineering 5. 51-75.

Ostendorp Wolfgang. 1995. Estimation of mechanical resistance of lakeside *Phragmites* stands. Aquatic Botany 51. 87-101.

SPM (Shore Protection Manual). 1984. Coastal Enginering Research Center.US Army Crops of Engineers.Washington.

Soulsby Richard. 1997. Dynamics of marine sands. Tomas Telford Publishing. London.

Teeter Allen M, Johnson Billy H, Berger Charlie, Stelling Guus, Scheffner Norman W, Garcia Marcelo H, Parchure T M. 2001. Hydrodynamic and sediment transport modelling with emphasis on shallow-water, vegetated areas (lakes, reservoirs, estuaries and lagoons). Hydrobiologia 444. 1-23.

Türker U, Yagci O, Kabdaşlı M S. 2006. Analysis of coastal damage of a beach profile under the protection of emergent vegetation. Ocean Engineering 33. 810-828

Widdows John, Brinsley Mary. 2002. Impact of biotic and abiotic processes on sediment dynamics and the consequences to the structure and functioning of the intertidal zone. Journal of Sea Research 48. 143-156.

Websites

Link 1- Morphometry of lake Krankesjön-Limnology at Lunds University
http://www.limnol.lu.se/kranke/page/maps.asp?map=1.

Appendix 1 – Significant wave heights and average periods at the deep water site

Table 1. Significant wave heights expected from the Rayleigh distribution and average periods at deep water site.

	Significant wave height Fixed station (*m*)	Average period Fixed station (*s*)	Significant wave height Movable station (*m*)	Average period Movable station (*s*)
Measurement cycle 1 (Movable station at pole 2)	0.0215	0.6228	0.0213	0.6207
Measurement cycle 1 (Movable station at pole 3)	0.0220	0.6102	0.0223	0.6250
Measurement cycle 1 (Movable station at pole 4)	0.0183	0.5538	0.0156	0.6316
Measurement cycle 1 (Movable station at pole 5)	0.0173	0.5625	0.0106	0.6977
Measurement cycle 1 (Movable station at pole 6)	0.0173	0.6040	0.0109	0.6950
Measurement cycle 1 (Movable station at pole 6)	0.0097	0.5678	0.0076	0.7087
Measurement cycle 1 (Movable station at pole 5)	0.0050	0.6429	0.0041	0.7087
Measurement cycle 1 (Movable station at pole 4)	0.0092	0.4580	---	---
Measurement cycle 1 (Movable station at pole 3)	0.0070	0.4523	0.0050	0.5438
Measurement cycle 1 (Movable station at pole 2)	0.0157	0.4675	0.0184	0.4972
Measurement cycle 2 (Movable station at pole 2)	0.0254	0.6360	0.0291	0.6545
Measurement cycle 2 (Movable station at pole 3)	0.0276	0.6818	0.0309	0.7317
Measurement cycle 2 (Movable station at pole 4)	0.0470	0.7287	0.0450	0.7595
Measurement cycle 2 (Movable station at pole 5)	0.0613	0.8333	0.0517	0.8955
Measurement cycle 2 (Movable station at pole 6)	0.0435	0.7860	0.0351	0.9137
Measurement cycle 2 (Movable station at pole 6)	0.0549	0.8531	0.0341	0.8824
Measurement cycle 2 (Movable station at pole 5)	0.0489	0.7826	0.0356	0.8491
Measurement cycle 2 (Movable station at pole 4)	0.0510	0.8531	0.0421	0.8257
Measurement cycle 2 (Movable station at pole 3)	0.0551	0.8451	0.0552	0.8867
Measurement cycle 2 (Movable station at pole 2)	0.0669	0.9137	0.0622	0.8571
Measurement cycle 3 (Movable station at pole 2)	0.0819	0.9574	0.0754	0.9836
Measurement cycle 3 (Movable station at pole 3)	0.0672	0.8411	0.0649	0.9184
Measurement cycle 3 (Movable station at pole 4)	0.0706	0.8780	0.0605	0.9375

Table 1. Continues…

	Significant wave height Fixed station (*m*)	Average period Fixed station (*s*)	Significant wave height Movable station (*m*)	Average period Movable station (*s*)
Measurement cycle 3 (Movable station at pole 5)	0.0689	0.9137	0.0514	0.9574
Measurement cycle 3 (Movable station at pole 6)	0.0698	0.9231	0.0433	0.9945
Measurement cycle 3 (Movable station at pole 6)	0.0757	0.9137	0.0410	0.9000
Measurement cycle 3 (Movable station at pole 5)	0.0847	1.0169	0.0531	0.9326
Measurement cycle 3 (Movable station at pole 4)	0.0831	0.9836	0.0648	0.8955
Measurement cycle 3 (Movable station at pole 3)	0.0722	0.9045	0.0760	0.9137
Measurement cycle 3 (Movable station at pole 2)	0.0677	0.8738	0.0644	0.9045
Measurement cycle 4 (Movable station at pole 2)	0.0616	0.9091	0.0644	0.8696
Measurement cycle 4 (Movable station at pole 3)	0.0655	0.8867	0.0583	0.9231
Measurement cycle 4 (Movable station at pole 4)	0.0660	0.8571	0.0540	0.8995
Measurement cycle 4 (Movable station at pole 5)	0.0605	0.8955	0.0465	0.9231
Measurement cycle 4 (Movable station at pole 6)	0.0604	0.8333	0.0423	0.9326
Measurement cycle 4 (Movable station at pole 6)	0.0680	0.9137	0.0444	0.9574
Measurement cycle 4 (Movable station at pole 5)	0.0613	0.8531	0.0478	0.9278
Measurement cycle 4 (Movable station at pole 4)	0.0779	0.9091	0.0627	0.8911
Measurement cycle 4 (Movable station at pole 3)	0.0633	0.8531	0.0607	1.0227
Measurement cycle 4 (Movable station at pole 2)	0.0634	0.8491	0.0569	0.8295
Measurement cycle 5 (Movable station at pole 2)	0.0358	0.7229	0.0322	0.7258
Measurement cycle 5 (Movable station at pole 3)	0.0495	0.7660	0.0428	0.7660
Measurement cycle 5 (Movable station at pole 4)	0.0416	0.8108	0.0370	0.8108
Measurement cycle 5 (Movable station at pole 5)	0.0359	0.7031	0.0330	0.8000
Measurement cycle 5 (Movable station at pole 6)	0.0372	0.7317	0.0266	0.7627
Measurement cycle 5 (Movable station at pole 6)	0.0355	0.7229	0.0298	0.7531
Measurement cycle 5 (Movable station at pole 5)	0.0335	0.7287	0.0284	0.7725
Measurement cycle 5 (Movable station at pole 4)	0.0359	0.7759	0.0377	0.8108

Table 1. Continues…

	Significant wave height Fixed station (*m*)	Average period Fixed station (*s*)	Significant wave height Movable station (*m*)	Average period Movable station (*s*)
Measurement cycle 5 (Movable station at pole 3)	0.0445	0.7595	0.0429	0.7531
Measurement cycle 5 (Movable station at pole 2)	0.0470	0.7595	0.0508	0.7930

Appendix 2 - significant wave heights and average periods at the beach

Table 1. Significant wave heights expected from the Rayleigh distribution and average periods at the beach.

	Significant wave height Fixed station (*m*)	Average period Fixed station (*s*)	Significant wave height Movable station (*m*)	Average period Movable station (*s*)
Measurement cycle 1 (Movable station at pole 2)	0.0818	1.0056	0.0755	1.0112
Measurement cycle 1 (Movable station at pole 3)	0.0574	0.9045	0.0569	0.9231
Measurement cycle 1 (Movable station at pole 4)	0.0657	1.0056	0.0624	0.9730
Measurement cycle 1 (Movable station at pole 5)	0.0583	0.8911	0.0574	0.9278
Measurement cycle 1 (Movable station at pole 6)	0.0625	0.9045	0.0657	0.9836
Measurement cycle 2 (Movable station at pole 2)	0.0837	0.9730	0.0812	0.9836
Measurement cycle 2 (Movable station at pole 3)	0.0824	1.0345	0.0776	1.0286
Measurement cycle 2 (Movable station at pole 4)	0.0930	1.0588	0.0841	1.0714
Measurement cycle 2 (Movable station at pole 5)	0.0984	1.0778	0.0932	1.1043
Measurement cycle 2 (Movable station at pole 6)	0.0984	1.0465	0.0892	1.0843
Measurement cycle 2 (Movable station at pole 6)	0.1006	1.1043	0.0925	1.1111
Measurement cycle 2 (Movable station at pole 5)	0.1108	1.2081	0.0956	1.1043
Measurement cycle 2 (Movable station at pole 4)	0.0990	1.0909	0.0948	1.1111
Measurement cycle 2 (Movable station at pole 3)	0.1012	1.1043	0.1000	1.1392
Measurement cycle 2 (Movable station at pole 2)	0.1066	1.0843	0.0998	1.0976

Appendix 3 – significant wave heights and average periods at the shallow water site

Table 1. Significant wave heights expected from the Rayleigh distribution and average periods at the shallow water site.

	Significant wave height Fixed station (*m*)	Average period Fixed station (*s*)	Significant wave height Movable station (*m*)	Average period Movable station (*s*)
Measurement cycle 1 (movable station at pole 2)	0.0873	1.1180	0.0819	1.1043
Measurement cycle 1 (movable station at pole 3)	---	---	---	---
Measurement cycle 1 (movable station at pole 4)	0.0831	1.0588	0.0696	1.0588
Measurement cycle 1 (movable station at pole 5)	0.0658	0.9326	0.0548	0.9574
Measurement cycle 1 (movable station at pole 6)	0.0802	1.0169	0.0601	1.1180
Measurement cycle 1 (movable station at pole 6)	0.0590	0.8867	0.0417	0.9184
Measurement cycle 1 (movable station at pole 5)	0.0759	0.9890	0.0608	0.9524
Measurement cycle 1 (movable station at pole 4)	0.0671	0.9626	0.0604	0.9677
Measurement cycle 1 (movable station at pole 3)	0.0623	0.9231	0.0637	0.9424
Measurement cycle 1 (movable station at pole 2)	0.0829	1.0588	0.0732	1.0526
Measurement cycle 2 (movable station at pole 2)	0.0791	1.0651	0.0777	1.0909
Measurement cycle 2 (movable station at pole 3)	0.0735	0.9783	0.0682	1.0405
Measurement cycle 2 (movable station at pole 4)	0.0859	1.0227	0.0738	1.0588
Measurement cycle 2 (movable station at pole 5)	0.0791	0.9890	0.0601	1.0651
Measurement cycle 2 (movable station at pole 6)	0.0796	1.0112	0.0571	1.0843
Measurement cycle 2 (movable station at pole 6)	0.0831	1.0405	0.0604	1.1180
Measurement cycle 2 (movable station at pole 5)	0.0869	0.9945	0.0675	1.1465
Measurement cycle 2 (movable station at pole 4)	0.0794	1.0405	0.0644	1.0078
Measurement cycle 2 (movable station at pole 3)	0.0949	1.0909	0.0790	1.0078
Measurement cycle 2 (movable station at pole 2)	0.0854	1.0345	0.0787	1.0405
Measurement cycle 3 (movable station at pole 2)	0.1066	1.1392	0.0964	1.1765
Measurement cycle 3 (movable station at pole 3)	0.1225	1.2245	0.1132	1.2414
Measurement cycle 3 (movable station at pole 4)	0.1142	1.1688	0.0953	1.1765

Table 1. Continues…

	Significant wave height Fixed station (*m*)	Average period Fixed station (*s*)	Significant wave height Movable station (*m*)	Average period Movable station (*s*)
Measurement cycle 3 (movable station at pole 5)	0.0909	1.0976	0.0781	1.2245
Measurement cycle 3 (movable station at pole 6)	0.0816	1.0843	---	---
Measurement cycle 3 (movable station at pole 6)	0.0646	0.9890	---	---
Measurement cycle 3 (movable station at pole 5)	0.0822	1.0651	0.0636	1.1111
Measurement cycle 3 (movable station at pole 4)	0.0899	1.0588	0.0837	1.1765
Measurement cycle 3 (movable station at pole 3)	0.0816	1.0227	0.0699	0.9626
Measurement cycle 3 (movable station at pole 2)	0.0685	1.0465	0.0735	1.0056